buildings

MDPI

Review

Test Procedures and Mechanical Properties of Three-Dimensional Printable Concrete Enclosing Different Mix Proportions: A Review and Bibliometric Analysis

Ghasan Fahim Huseien [1,2,*], Shea Qin Tan [2], Ali Taha Saleh [3], Nor Hasanah Abdul Shukor Lim [2] and Sib K. Ghoshal [4]

[1] Guangzhou Institute of Energy Conversion, Chinese Academy of Sciences, Guangzhou 510640, China
[2] UTM Construction Research Centre, Institute for Smart Infrastructure and Innovative Construction, Faculty of Civil Engineering, Universiti Teknologi Malaysia, 81310 Johor Bahru, Johor, Malaysia; sqtan5@graduate.utm.my (S.Q.T.)
[3] Department of Chemistry, College of Science, University of Misan, Amarah 62001, Iraq; alitaldosari@uomisan.edu.iq
[4] Department of Physics and Laser Centre, AOMRG, Faculty of Science, Universiti Teknologi Malaysia, Skudai 81310, Johor, Malaysia; sibkrishna@utm.my
* Correspondence: eng.gassan@yahoo.com; Tel.: +65-83057143

Abstract: Three-dimensional printable concrete (3DPC) has become increasingly popular in the building and architecture industries due to its low cost and fast design. Currently, there is great interest in the mix design methods and mechanical properties of 3DPC, particularly in relation to yield stress analysis. The ability to extrude and build 3D-printed objects can be significantly affected by factors such as the rate of extrusion, nozzle size, and type of pumps used. It has been observed that a yield stress lower than 1.5 to 2.5 kPa is not sufficient to maintain the shape stability of concrete, while a yield stress above this range can limit the material's extrudability. Furthermore, the strength properties of 3DPC are influenced by factors such as changes in yield stress and superplasticiser dosages. To meet the high mechanical strength and durability requirements of 3DPC in the construction industry, it is essential to analyse the material's early-age mechanical properties. However, the development of standardised test methods for 3DPC is still deficient. To address this issue, a bibliometric analysis was conducted to comprehensively review the diverse test methods and mechanical characteristics of 3DPC with different mix proportions. To produce high-performance concrete from various additives and waste materials, it is critical to have a basic understanding of the hydration processes of 3DPC. Moreover, a detailed analysis of the environmental impact and energy efficiency of 3DPC is necessary for its widespread implementation. This review article will highlight the recent trends, upcoming challenges, and benefits of using 3DPC. It serves as a taxonomy to navigate the field of 3DPC towards sustainable development.

Keywords: 3DPC; digital concrete; buildability; extrudability; robustness; mechanical properties; test procedures; bibliometric analysis; environmental sustainability

check for updates

Citation: Huseien, G.F.; Tan, S.Q.; Saleh, A.T.; Lim, N.H.A.S.; Ghoshal, S.K. Test Procedures and Mechanical Properties of Three-Dimensional Printable Concrete Enclosing Different Mix Proportions: A Review and Bibliometric Analysis. *Buildings* **2024**, *14*, 2667. https://doi.org/10.3390/buildings14092667

Academic Editor: Bo-Tao Huang

Received: 16 June 2024
Revised: 29 July 2024
Accepted: 22 August 2024
Published: 27 August 2024

Copyright: © 2024 by the authors. Licensee MDPI, Basel, Switzerland. This article is an open access article distributed under the terms and conditions of the Creative Commons Attribution (CC BY) license (https://creativecommons.org/licenses/by/4.0/).

1. Introduction

Over the years, although construction has been recognised as a conventional industry, it has lagged behind other sectors in terms of automation and advanced technology implementation [1,2]. It is acknowledged [3,4] that several industries, like consumer product, automobile, and aerospace industries, have intensively exploited various automation and the latest technologies to improve productivity significantly. Thus, cementitious material management is the scientific foundation of innovative construction. In recent years, several novel digital and automation-based methods have been developed for improved construction [5,6]. Khoshnevis [7] developed the method of contour crafting and used

the technology in the early work of the construction industry [7–9]. Its development was stable and continuous, but the development of this technology has increased rapidly since 2012. According to [2,10,11], the rapid progress of digital and information science in recent years provided an impetus to structural engineering that eventually evolved into digitised and automated 3D printable concrete (3DPC). Tay et al. [10], De Schutter et al. [12], and Wangler et al. [13] showed that 3D printing technology has generated much interest in construction industries worldwide.

Digital fabrication with concrete is one of the techniques employed in manufacturing 3D printable concrete and is capable of proficiently and rapidly generating architectural or structural components without formworks and contributes to improvements in construction cost administration, security, and sustainability [14–16]. A preservative fabrication method in which a structure is constructed level by level according to a predetermined three-dimensional computer prototype is one of the 3D printing technologies. The authors of [17–19] made a layer-wise accumulation of materials to create a structure according to a CAD model and analysed the possibilities of 3DPC in the construction industry. Meanwhile, preservative fabrication is an approach that utilises 3D CAD models to construct an actual substance [20]. Rahul et al. [18] used a set of computer G codes to create a prototype for the initial printing of a substance. Then, the printed material was squeezed out by the print route-based print head determined by the G codes in a standard 3D printing procedure. Thus, 3D concrete printing can extrude cementitious ingredients to construct substances in a level-by-level approach [21–23]. Consequently, concentrating on layered extrusion manufacturing processes, such as contour crafting and 3D concrete printing, a fresh and viscous cementitious composite in the form of deposits normally extrudes from the moving head of automated printing apparatus, resulting in a digitalised track of a solid separated into some portions [10,24,25]. Each portion has a predefined width that is repeatedly positioned onto the former level to complete the process, thereby making the end product.

Construction using 3DPC has countless advantages compared to traditional technology. These include skilled workforce reduction, a decrease in raw materials used, and easy printing of complex structures in the absence of any formworks [24–27]. In addition, a variety of opportunities and technological advancements is launched by digital construction that is independent of formwork, imparting high geometrical flexibility, extra functions, and a significant reduction in outlay and time, thus lessening dependence on skilful manpower [27–30]. According to the studies of Buswell et al. [27] and Lim et al. [24], such a method of construction excludes the need for formwork since the concrete can self-assist. It also proposes good capability in the sense of time-conserving and offering design and geometric elasticity. Therefore, the main proposition and innovative prospects of digital concrete may offer an immense contribution to 4G construction industries. This digital concrete not only brands construction as a fully digitalised, all-in-one process but also characterises a decision-making and rational attempt from well-established digital technologies and designs (CAD and BIM) towards digital industrialisation or manufacturing [5].

In terms of the engineering properties of cementitious material, pumpability, extrudability, and buildability are the fundamental requirements for selective material depositions by extrusion [5]. Pumpability defines the simplicity of transferring a fresh mixture from the pumps to the extrusion nozzles [31] and is identified as the simplicity of transferring the ingredient from the source to the nozzle [21]. The pumping of concrete ingredients is a complicated process due to not only its time-dependent material performance but also variations in the concrete characteristics caused by the pumping requirements, like bleeding and segregations, that may affect the pumping process of the ingredient and are difficult to forecast [32]. Therefore, acceptable pumpability should be considered so that fresh concrete can be transported uninterruptedly but still determined by other considerations, such as concrete's plastic viscosity or greasing coating development [33,34].

Extrudability signifies the simplicity of constantly squeezing out an ingredient at a provided flow speed, but still, it relies on the rheology of fresh mortars and the extruder

or print-head design. The authors of [31,35] stated that extrudability can be defined as the capability to squeeze out the composite by a plunger with insignificant cross-section distortion and a tolerable level of shredding of the filaments. As a result, fresh 3D printable concrete should have appropriate extrudability for passing through the printer nozzles [35]. After the concrete is extruded from the nozzle, there is a possibility that the paste may be separated from the aggregate, resulting in the obstruction of the tube. Inadequate particle size distribution or an excessive water-to-binder ratio are the primary triggers that contribute to this phenomenon [36]. In an appropriately designed mixture, sufficient leftover paste contents must exist to fill up the spaces amid the aggregates. This paste content develops a coating that wraps up the aggregates and serves as a "lubricant" between the aggregates when shear stress is employed in the mixture [37]. The frictional force among these aggregates is reduced, and the mix workability is improved due to the lubricant effect of the paste [38].

According to Nerella et al. [5], buildability is characterised as the capability of an extruded cementitious ingredient to maintain its geometry structure and volume under continuous and escalating burdens in a fresh state, which correlates with the definition given by [39]. It is inferred that the printed filament must be produced with minimum distortion when subjected to successive levels of load. Lim et al. [24] defined buildability as the endurance of the accumulated fresh ingredient to distortion under weight. Buildability is defined by Kazemian et al. not only as the capability of an extruded ingredient to maintain its geometry figure and dimension under continuous and cumulative weights [5] but also as the capability to withstand distortions during deposit-wise concrete production [10]. Buildability depends on the composite yield stress, strength of the structure, and level of cross-section shape-related figure reliability. The structural build-up of concrete mixes strongly depends on the flocculation and hydration reaction rates [40]. Compared to the structure gain speed of the mixes, if the accumulation of the successive level is faster, then the composition may collapse [41]. The equilibrium amid the structure build-up rate of the mixes and printing constraints is crucial to accomplish high buildability. The material structural build-up rate can be enhanced by the addition of admixtures, such as accelerators [42]. The time-dependent increase in the squeezed-out mixes yields stress and mainly depends on the flexible physical alterations in the structure as a result of thixotropy and permanent structural alterations as a result of cement hydration [43]. Therefore, 3DCP with enhanced buildability achieves higher yield stress. Nevertheless, the extrudability of a mix may drop due to it being too stiff to print if the yield stress of concrete is too high.

To provide a comprehensive taxonomy regarding the advancement of 3DPC, a bibliometric analysis was conducted wherein the current trend of this novel construction component was emphasised (Figure 1). Bibliometric analysis is a type of study for mining valuable data in a field and enables one to collect data for the improvement of various research domains in human endeavours. In essence, this analysis accommodated numerous studies, which were not only used to measure the influence of authors, articles, journals, institutions, and the most contributing countries but also included the publication and citation trends in the area of 3D printable concrete. According to Chadegani et al. [44], there are two major databases useful for a comprehensive overview of the State-of-the-Art literature, including Scopus and the Web of Science (WoS), wherein the former is wider and contains more recent research. This paper implemented Scopus as the main data resource because WoS offered nearly 500 documents on 3DPC per download. Conversely, Scopus allowed more than 2000 documents on 3DPC per download, thus it was selected as the primary database for bibliometric analysis and visualisation.

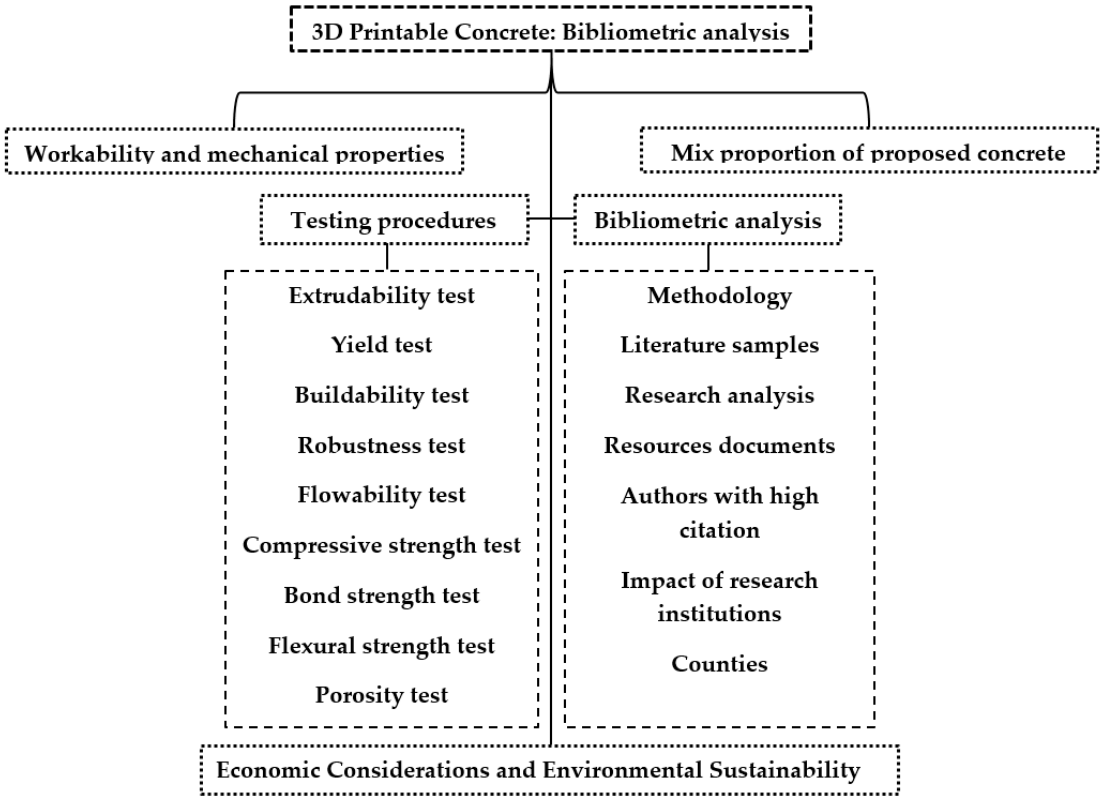


Figure 1. Flow chart of bibliometric analysis study for 3D printable concrete.

2. Mix Proportions

In the mix designs of 3DPC, various types of additives and admixtures are usually implemented. For example, mixes containing fluctuating hydroxypropyl–methyl cellulose (HPMC) were utilised by Srinivasan et al. [45]. They found that the pressure increased continuously without HPMC because water was pressing out from the mixture, whereas the pressure was low and stayed constant with increasing amounts of HPMC. Kuder and Shah [46] discovered that a minimal quantity of HPMC or a mixture of calcined clay (CC) and methyl cellulose (MC) may be essential for productive extrusion. In the study of Tregger et al. [47], the influence of CC, fly ash (FA), and superplasticisers on cement paste strength properties was investigated. The researchers observed a decrease in yield stress (Ty) when both FA and superplasticisers were added, but an increase in Ty when CC was added (as shown in Table 1). Another study by Peled et al. [48] looked at how the addition of FA affected the rheological extrudable fibre mixes and found that adding FA together with acrylic and polyvinyl alcohol fibres resulted in a decrease in extrusion pressure. However, FA addition did not change the extrusion pressure with glass fibre addition, while the FA supplement improved it with the cellulose fibre addition. Voigt et al. [49] studied the impact of FA and CC on the designed fresh composite's stability and flow, wherein it was observed that the addition of FA could enhance the flowability and reduce the shape stability of mixes. In contrast, the supplement of CC could enhance the shape stability and slightly reduce the flowability, depending on the nature of the CC. In short, the blending of FA and CC was asserted to be advantageous in producing mixes with high flowability and requiring shape stability. Rahul et al. [18] studied the yield stress of mixes designed with Portland cement appropriate for extrusion. It was shown that the addition of superplasticisers could reduce the stability and robustness of composites that were only printable for 15 min. However, the addition of nanoclay could enhance both the robustness and stability of the mixture. Furthermore, the yield stress was improved when the content of nanoclay was raised. The supplement of a viscosity-modifying agent and silica fume also led to a robust and stable composite (Table 2).

Table 1. Shear rheology of the mix design [47].

Mixes	Yield Stress (Ty)		Volume Fraction (Φ)		
	Ty [Pa]	*Ty* [psf]	Φ Min.	Φ Max.	Φ Different
Cement	76.32	1.59	0.523	0.570	0.0465
High-range water-reducer	62.24	1.30	0.516	0.591	0.0750
Fly ash	34.76	0.73	0.494	0.579	0.0853
Clay 1	97.31	2.03	0.520	0.546	0.0255
Clay 2	80.65	1.68	0.522	0.549	0.0268
Clay 3	89.02	1.86	0.516	0.556	0.0397

Table 2. Buildability and extrudability of concrete [18].

Mixes	SP Dosage (%)	Buildability of Comp. of Bottom Layer, mm	Extrudability	Yield Stress, kPa	Flow Value, %
Silica fume	0.19	2 ± 0.5	Pass	1.1 ± 0.1	97 ± 10
	0.18	0	Pass	1.5 ± 0.2	89 ± 10
	0.17	0	Pass	1.6 ± 0.3	80 ± 5
	0.16	0	Fail	2.6 ± 0.3	55 ± 5
Nanoclay	0.15	2 ± 0.5	Pass	1.1 ± 0.1	115 ± 15
	0.14	0	Pass	1.5 ± 0.2	100 ± 10
	0.13	0	Pass	1.6 ± 0.2	95 ± 10
	0.12	0	Pass	2.3 ± 0.3	90 ± 10
	0.11	0	Fail	2.9 ± 0.3	60 ± 5
Viscosity-modifying agents	0.20	2 ± 0.5	Pass	1.3 ± 0.1	100 ± 10
	0.19	0	Pass	1.5 ± 0.2	88 ± 10
	0.18	0	Pass	1.6 ± 0.2	80 ± 5
	0.17	0	Pass	2.0 ± 0.2	70 ± 5
	0.16	0	Pass	2.5 ± 0.3	65 ± 5
	0.15	0	Fail	3.0 ± 0.4	40 ± 5

An additional important feature of printable composites is the structural build-up caused by thixotropy and cement hydration. Quanji et al. [50], who examined the outcomes of attapulgite clay on thixotropy, as shown in Figure 2, and the rate of cement hydration, detected that nanoclay addition enhanced the rate of hydration and the area enclosed in the hysteresis loop at the same time. Comparable outcomes on cement hydration were also detected by Heikal and Ibrahim [51]. They proved that the initial and final setting times of cement paste decreased with the supplement of nanoclay. In addition, Qian and Schutter [52] revealed that the dynamic yield stress, thixotropic index, and the size of flocs developed in fresh cement paste improved with the add-on of attapulgite clay. Next, Rahul et al. [17] showed that a composite with viscosity-modifying agent addition had the slowest structural build-up, whereas a composite with silica fume addition displayed the fastest structural build-up. Compared to viscosity-modifying (VM) agents [15], the inclusion of nanoclay (NC) and silica fume (SF) significantly led to reducing the initial setting time from 252 min to 165 and 142 min and the final setting time from 476 min to 360 and 298 min, respectively. This is due to the time constraints of printability for the composites consisting of silica fume, nanoclay, and a viscosity-modifying agent, which were 30, 30, and 45 min, respectively. Therefore, the slow structural build-up noticed in the composite with viscosity-modifying agent addition resulted in longer time constraints of printability. Despite some research on the impact of viscosity-modifying agents on the thixotropy of ce-

ment paste, there is still a lack of sufficient studies in this area. Assaad et al. [53] found that the addition of polysaccharide-based polymers improved the thixotropy of self-compacted concrete, while Knapen and Van Gemert [54] showed that the use of various cellulose ether-based polymers extended the inactive period of cement hydration.

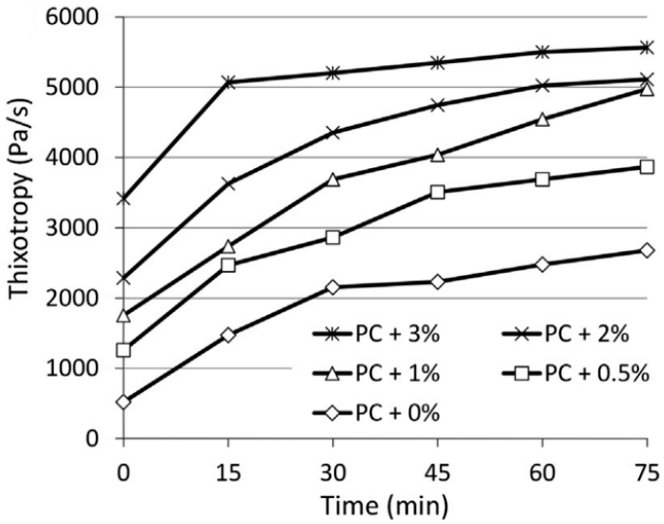


Figure 2. Effect of nanoclay content on the time-dependent rheological behaviour of cement paste thixotropy [50].

Several studies have recommended evaluating the fresh characteristics of 3DPC. Yossef et al. [55] categorised four parameters, extrudability, workability, open time, and buildability, as important factors in determining the properties of 3DPC mixes. Kazemian et al. [2] used printing windows, printing quality, and shape stability as necessary factors to determine the properties of 3DPC composites. Previous research [4,16,22] on various mix designs has shown that incorporating silica fume and ultrapure attapulgite clay enhances the shape stability of the printable layer. Furthermore, a slight improvement was observed with the inclusion of polypropylene fibres in concrete mixtures.

3. Fresh and Hardened Properties

3.1. Fresh Properties

The technique of constructing layer by layer in 3DPC requires the rapid development of compressive strength in order to bear the stress from the layers above. Previous research has varied the initial setting time of samples between 30 and 120 min to achieve early compressive strength [11,56,57]. Although the strength of samples gradually increases in the early stage of development, the samples may still experience significant deformation, causing the stress–strain curve to resemble a hill, as illustrated in Figure 3. The failure mode is similar to that of plastic materials, where the cross-sectional area expands as vertical deformation increases. As hydration progresses over time, the growth of compressive strength accelerates. The strength continues to increase until it reaches a peak value, after which it decreases, indicating the brittle failure behaviour of concrete [58–67].

At the early stage, the shear stress of 3DPC exhibits a similar trend to the compressive strength, with equal development rates. The elastic modulus and cohesion increase linearly with age, while the Poisson's ratio and angle of internal friction remain constant [11]. Additionally, fresh 3DPC is at risk of experiencing plastic cracking due to inadequate curing, especially in severe environments, such as hot and windy conditions [59,60]. Moelich et al. [60] observed that cracks formed within 2 h after extrusion, which is earlier than conventional concrete. Typically, plastic shrinkage occurs due to the rapid evaporation of water from the concrete surface, leading to shrinkage stress. As a result, plastic cracks appear when the shrinkage stress exceeds the corresponding tensile stress, which is typically low for fresh concrete.

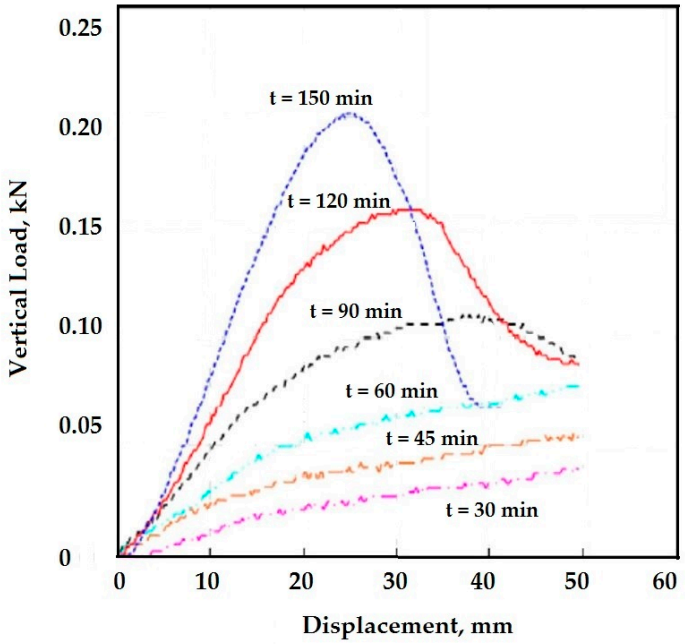


Figure 3. Stress–strain curve in fresh state [67].

3.2. Hardened Properties

Numerous studies have been conducted to determine the mechanical performance of 3DPC. Tran [61] demonstrated that 3DPC might have anisotropy. In addition, it was shown that mould-cast concretes have higher compressive strength (CS) and flexural strength (FS) compared to printed specimens. This might be due to the compressive and flexural strengths of printed specimens being dependent on the loading direction. The existence of cavities at the intersection between four filaments was also noticed when a circular plunger was utilised. This observation is also confirmed by Rahul et al. in [17,18], wherein the development of test methods was applied to describe the strength performance of 3D printable wall components. The presence of the high porosity of 3DPC at the horizontal and vertical layer interfaces was higher than the mould-cast concrete, causing lower bond shear strength at the contact surfaces than the mould-cast concretes. However, the higher value of bulk flexural stress of 3DPC was due to lower porosity than the mould-cast specimen. Tay et al. [10] made similar observations in the values of CS and FS for 3DPC and mould-cast geopolymer specimens.

With the increase in time difference between layers, the printing rate or height of the plunger from the accumulated layer was found to reduce the tensile bond strength. Nerella et al. [30] obtained the opposite results to Rahul et al. [17] and Tay et al. [10]; they realised that printed specimens showed roughly 10% higher CS compared to mould-cast specimens when examined along particular directions. These inconsistent findings obtained by previous researchers indicate that the mechanical characteristics may be influenced by different aspects, such as the types of mix designs, printers, and printing considerations applied in some studies. Roussel [62] evaluated the interface strength under conditions where the layers were safeguarded from drying up and subjected to drying. The results determined that the contact surface strength decreased to a maximum of 50% when the printed layers were subjected to dehydration. Srinivasan et al. [45] obtained similar results wherein it was argued that the elimination of surface moisture caused by evaporation could trigger bond strength reduction. In addition, heat curing is one of the factors causing water evaporation from the concrete mix, which most likely affects strength reduction by forming weak interlayer bonding in the mixtures. Therefore, optimal and precise material design and curing conditions are required to attain long-term performance and durability [63]. Table 3 shows the summary of results on compressive strength and flexural strength conducted according to various standards from different literature reviews.

Table 3. Hardened properties from different literature reviews.

Type of Binder	CS (MPa)	FS (MPa)	References	Standard
Portland cement, silica fume	49.9	-	[2]	[68]
Portland cement, fly ash, silica fume	71.7	-	[17]	[68]
Portland cement, fly ash, silica fume	61	11	[18]	[68]
Portland cement, fly ash, silica fume	107	11	[39]	[69]
Portland cement, nanoclay	97.9	-	[51]	[70]
Portland cement, fly ash, silica fume	110		[64]	[69]
Portland cement, fly ash, silica fume	53.2	7.8	[65]	[71]
Portland cement, fly ash, slag	31	4.3	[66]	-

4. Testing Procedures

4.1. Extrudability Test

Rahul et al. [17] described the extrudability of concrete as the capability to squeeze out the mixture constantly via the printer outlet with the necessary dimensional consistency, thereby developing layers with excellent printing quality. The extruded components removing the imperfections, such as cavities and incoherence, were considered for excellent print quality. The quality of these layers was determined through visual inspection. The dimensions of a single layer of extruded material were measured using a test bed printer. The measurements were taken at 10 cm intervals along the 30 cm length of the printed line. The extruded layer was considered to have passed the test if the dimensions at all measurement points were similar to those obtained for a rectangular plunger with dimensions of 30 mm $\times$ 20 mm $\pm$ 0.5 mm, and the printed layer had a smooth surface without any imperfections. A similar experimental procedure was conducted by Le et al. [64], where the ability to extrude was assessed by creating 9 mm-wide filaments using a 9 mm nozzle. Five groups of filaments were evaluated, as depicted in Figure 4. Each filament was 300 mm long, and the total length of filaments used in the test was 4500 mm. The test shape was designed to simulate the typical construction of freeform components. The test results were classified as either YES or NO, with YES indicating that all 4500 mm of filament was successfully deposited without blockage or fracture.

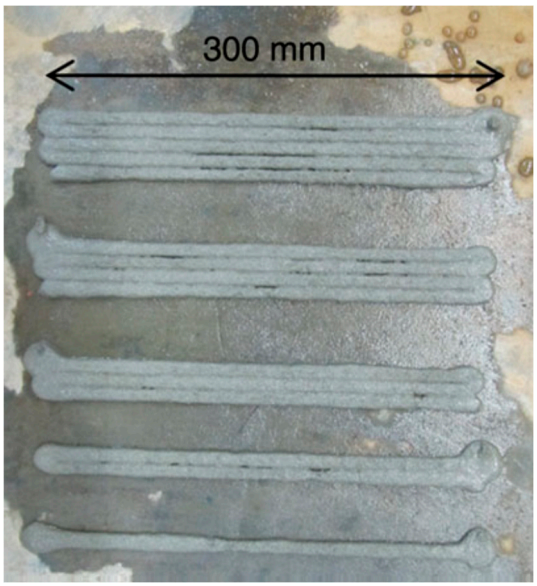


Figure 4. Extrudability test procedure [64].

A slight modification was carried out by Ma et al. [65] on the extrudability parameter, where the extruded filament from a printing nozzle with an aperture of 8 × 8 mm^2 was tested for continuity and stability to evaluate the extrudability of fresh paste. This nozzle aperture was one-third the size of the standard 8 × 24 mm^2. Each filament was meant to have a total continuous length of 2000 mm, which was accomplished using eight return procedures, with each subsection measuring 250 mm in length.

4.2. Yield Stress

Rahul et al. [18] directly measured the yield stress via the stress development test using a soil vane shear setup. A four-bladed vane with a diameter of 12 mm and a height of 24 mm was utilised (Figure 5). For this stress development test, the mixture was exposed to a uniform strain change. The yield stress was obtained by converting the recorded maximum torque value via the Dzuy and Boger equation, as shown in Equation (1) [18].

$$T = \frac{\pi}{2} D^3 \tau_y \left(\frac{H}{D} + \frac{1}{3} \right), \quad (1)$$

where T is the measured maximum torque (Nm), τ_y is the yield stress (N/m^2), H is the height (m), and D is the diameter of the vane (m).

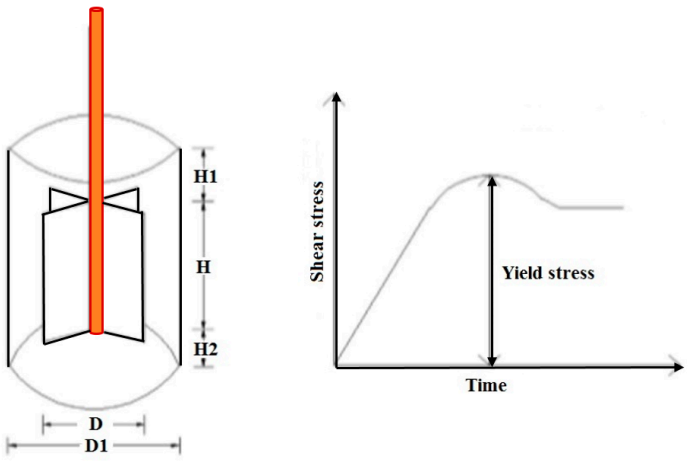


Figure 5. Vane shear test [18].

In this measurement, the tested specimen was instantly relocated to a cylindrical vessel (with a diameter of 5 cm and a height of 7.5 cm) after mixing. As illustrated in Figure 1, the vane was then implanted into the vessel at heights of H1 = 3 cm and H2 = 2.1 cm. All specimens were allowed to rest for about 3 min prior to the beginning of the test to obtain results with higher consistency. Then, the specimen was revolved at a fixed minimum speed of 0.1 rpm to obtain the highest torque. A low rpm of the vane shear apparatus was chosen to be applied in this test because the validity of the conversion relationship is only at a minimal speed, as the yield stress may be overestimated at a higher rpm. It is worth noting that the specimens were thixotropic, with a prehistory-dependent reaction. Identical procedures were followed for all specimens and repeated using different specimens to guarantee duplicability.

4.3. Buildability Test

Following the procedure recommended by Kazemian et al. [2], Austin et al. [67], and Zhang et al. [72], the buildability test was carried out to evaluate accumulated layer buildability. In the research of Kazemian et al. [2], the concrete samples were printed in two layers at different times. The CS of the underneath layer was defined after the next layer was printed. The time gap was defined according to the element to be printed. Austin et al. [67] and Zhang et al. [72] mentioned that the capacity of fresh concrete to be

built up was measured by determining the number of layers of filaments that could be added without causing noticeable collapse or deformation of the lower layers based on the same shape used in evaluating extrudability. Rahul et al. [18] assessed the structural build-up of concrete using penetration testing following ASTM C403/C403M [73] and a cement hydration rate test by semi-adiabatic calorimetry in accordance with BS EN 196-9 [74]. The sample was moulded in a cylinder 80 mm in diameter and 165 mm in height, followed by a semi-adiabatic calorimetry test. The temperature was increased for the duration of 72 h. The printable time period signified the maximum duration through which the mixture could pass the extrudability test.

A similar concept of a buildability test procedure is mentioned in the study of Ma et al. [65]. To construct layered structures, the combined paste is kept in a reservoir and extruded via a nozzle. These constructions are made up of twenty vertically stacked layers of extruded filaments that are each 250 mm long and 30 mm wide. They must be able to maintain their form for at least 10 min without collapsing. This 10 min rest period is meant to evaluate the shape retentivity and load sustainability of various tailing materials while preventing cold joints and weakening interfaces. Each layer is intended to be 8 mm tall, allowing the machine to go up in 8 mm increments.

4.4. Robustness Test

Rahul et al. [18] suggested the need to produce a steady and strong mixture proportion with low flexibility in yield stress, especially for industrial applications. To measure robustness, the high-range water-reducing admixture dosage equivalent to the necessary yield stress (YS) was altered by ± 0.01 and $\pm 0.02\%$. The difference in yield stress from the allusion value in terms of the variability factor (V) was calculated using Equation (2):

$$TV = \sqrt{\frac{\Sigma \left(YS - YS_{ref} \right)^2}{N}} \quad (2)$$

where YS_{ref} is the yield stress of the reference mixture, YS is the corresponding yield stress obtained for each variation in the high-range water-reducing admixture dosage, N is the number of specimens, and V is a degree of changes in yield stress from its needed value with regard to the difference in the high-range water-reducing admixture dosage. A mixture with lower sensitivity and stability will have a lower value of V.

4.5. Flowability Test

The flowability test was performed to evaluate the flow values of 3DPC. The slump and slump-flow tests were conducted in accordance with ASTM C230/C230M [75], as referred by Tay et al. [21]. The specification for the flow table test followed ASTM C1437 [76], as recommended by Rahul et al. [18]. The flow table test was considered to measure the flowability of prepared mixtures, in which the flow table was cleaned and dried before being placed in the flow mould at the table centre. First, a 25 mm-thick mortar layer was filled in the mould, followed by tampering about 20 times, ensuring a homogeneous filling. Next, the second layer was filled in the mould and tampered like the first layer. The mortar was sliced to a planer surface flushed with the mould top by drawing a straight or trowel edge with a sawing movement across the mould top. Again, the tabletop was cleaned and dried to eliminate any residual water from the flow mould edges. Later, the mould was lifted away from the mortar 1 min after the completion of the mixing process, followed by immediate dropping of the table 25 times in 15 s. Thereafter, the mortar diameter was measured, and the flow was computed in percent by dividing the average of four readings minus the original inside base diameter (A in millimetres) over the original inside base diameter (in millimetres) and multiplying by 100.

4.6. Compressive Strength Test

Casagrande et al. [77] tested cylindrical samples under displacement control at room temperature using an MTS electromechanical Universal Testing Machine of a 10 kN capacity. The test was performed to the highest vertical strain of 12%, with a displacement of 15 mm. Due to the difficulty in observing the physical properties of the specimen with no changes, the stress and strain values were obtained from the measured force versus the displacement plot. The reduction modulus obtained from strains varied from 0 to 2%, and Young modulus was calculated. However, it was essential to launch a dependable strategy to recognise the acceptable varieties of Young modulus measurement because the strain might have been modified based on the features of the printing materials. Usually, these tests are performed at extremely low-load-level commands, particularly at a very early age, wherein minor differences in the material composition, like the mix design and environmental conditions, could make a notable stiffness change. In addition, the values of Young modulus might have depended on the details of the test used for approximating the strain values. The time-dependent stress–strain development was obtained from the compressive test at various concrete ages, with a deformation rate of 3 mm/min. The mechanical characteristics of hardened and fresh mixes were found to be rate-sensitive, enhancing the strength with the increase in strain rate. The compressive test at a higher displacement rate was only conducted for the reference mix to only examine one irregularity in a period, but this rate remained within the displacement rate limit, which is presently applied to test printable mortars.

As illustrated in Figure 6, the study conducted by Rahul et al. [17] evaluated the CS of a total of six cubes of printed concrete with the dimensions of 50 mm × 50 mm × 50 mm slashed from wall components at different loading directions. Figure 7 shows the positions for the removal of the cubes. In addition, a 5 mm piece was eliminated from both sides of the cubes to attain a width of 50 mm. In order to obtain loading along D1, D2, and D3 directions, positions 1 and 4, 2 and 5, and 3 and 6 were used, respectively. The procedure was repeated to obtain a total of 12 cubes with the dimensions of 50 mm × 50 mm × 50 mm in the three selected directions of loading, followed by standard mould casting. The loading rate and test procedure for both cubes (printed and mould-cast) were performed in accordance with ASTM C109/C109M [68].

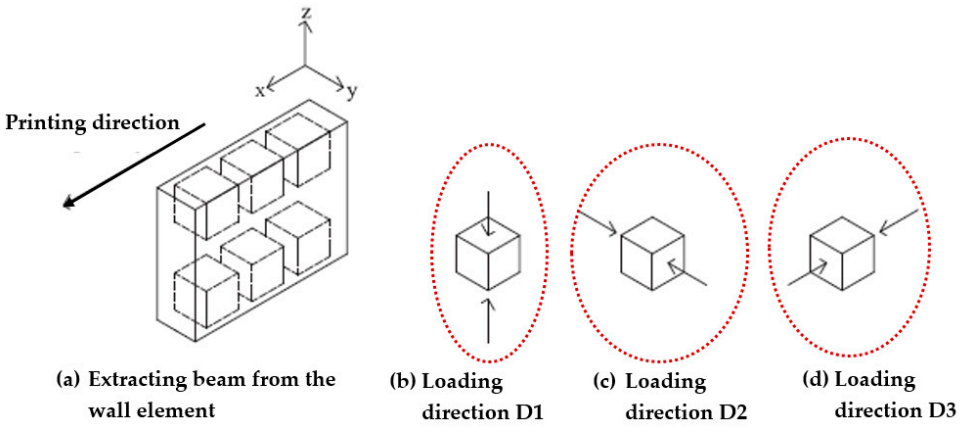


Figure 6. Various loading directions for CS test [17].

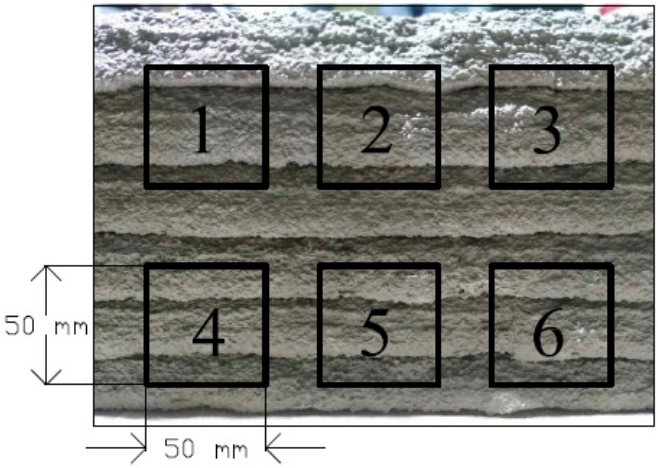


Figure 7. Cube removal from the wall component for CS test [17].

4.7. Porosity Evaluation

Rahul et al. [17] determined the porosities of mould-cast and printed concrete sized 20 mm × 10 mm × 10 mm. For the former specimen, the samples were sliced off from cubes 50 mm × 50 mm × 50 mm in size, and a total of four samples were tested to obtain the mean value. The two printed concrete wall models were printed to extract two specimens from locations 1 to 6 (Figure 8). Their porosity was evaluated at the bulk, horizontal, and vertical position borderlines of the wall component. For the evaluation of the porosity of bulk specimens, these samples were extracted vertically from locations 3 and 4. Conversely, for the evaluation of porosity at the borderline amid two horizontal layers, the samples were removed vertically from positions 1 and 2. Furthermore, for the evaluation of porosity at the borderline amid two vertical layers, the samples were removed horizontally from positions 5 and 6. The vacuum saturation approach was used to examine the porosity of all oven-dried (at 50 °C for one week) specimens. The specimens were stored in the vacuum desiccators for 3 h to eliminate surplus humidity and cool down to room temperature. Next, the samples were submerged in desiccators containing calcium hydroxide solution and kept in a vacuum environment. After an hour, the vacuum was freed under submerged conditions for 18 h. The vacuum-saturated porosity (ρ) of specimens was calculated using Equation (3):

$$\rho = \frac{M_1 - M_2}{M_1 - M_3} \times 100 \quad (3)$$

where M_1, M_2, and M_3 are the corresponding sample weights saturated in air, dried in air, and saturated in water.

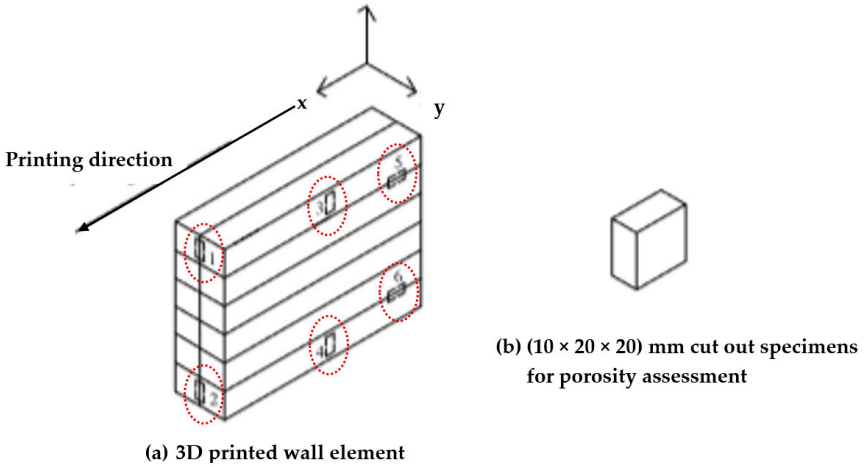


Figure 8. Sample extraction from wall component to evaluate the porosity [17].

4.8. Bond Strength Assessment

Rahul et al. [17] used cylindrical samples (removed from the wall component) 25 mm in diameter and 40 mm in height to evaluate the bond strength (Figure 9). Six samples in the form of cylinders were extracted horizontally from positions 1 and 2, and six samples were extracted vertically from positions 3 and 4 to illustrate the contact surfaces amid the horizontal layers. The bond strength of the mould-cast specimen of the dimensions 50 mm × 50 mm × 50 mm was obtained by slashing out the cylindrical samples. A direct bond shear test (a Zwick Roell machine equipped with a load cell of 5 kN) was carried out to examine the extracted material strength (Figure 10). The cylindrical samples were positioned horizontally in the channels of the upper and lower jaw due to the occurrence of borderlines in the middle. Then, the jaws were ripped apart at a uniform rate of displacement (0.1 mm/min). The bond shear strength was calculated by dividing the failure load by the cross-sectional area of the cylinder. To determine the bond strength of the mould-cast specimen, the same procedure was repeated by applying the cylindrical samples extracted from mould-cast cubes.

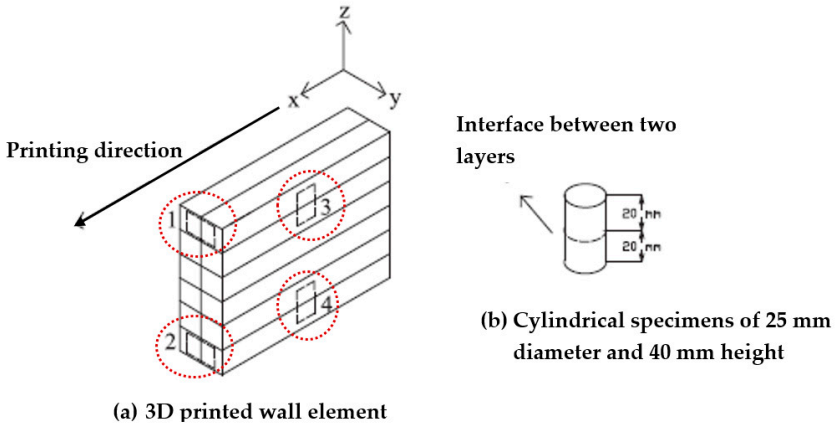


Figure 9. Bond shear testing on the samples extracted from the wall component [14].

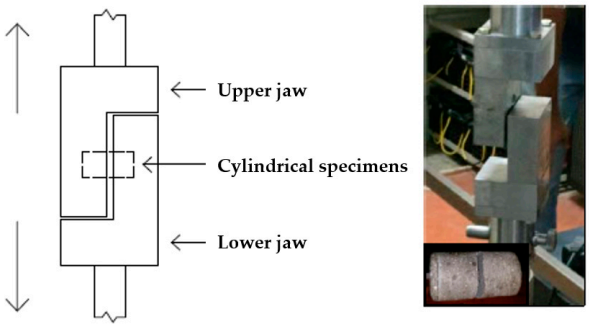


Figure 10. Zwick Roell testing machine [17].

4.9. Flexural Strength Evaluation

Using the three-point bending test, Rahul et al. [17] assessed the FS of concrete beams (mould-cast and printed) with the dimensions of 160 mm × 40 mm × 40 mm. These concrete beams were cast in standard moulds. The beams of printed specimens were extracted from three separate positions (Figure 11). A portion of 10 mm was sliced off from both sides of a wall component 60 mm in size to obtain a beam width of 40 mm for testing (Figure 12). When exposed to horizontal loading, a beam extracted vertically from location 1 experienced bending in the upright plane (Figure 12b), symbolised as E1 direction for reference. When the beam was exposed to a horizontal load, the sample cut off from locations 2 and 3 was tested in a horizontal section (Figure 13b) and denoted as E2 direction. In addition, the beams cut off from positions 2 and 3 were examined along E3 (Figure 13c) under vertical loading. A total of 12 wall components were printed, and three

beams were cut off from each of them (Figures 12a and 13a). There were 12 vertical beams extracted from position 1 for testing with loading along E1, while six beams extracted from positions 2 and 3 were tested with loading along E2 and E3. The FS test was performed according to ASTM C 348 [78].

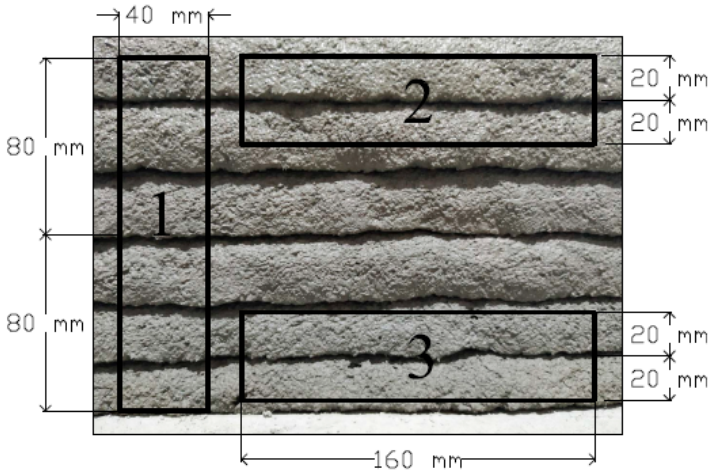
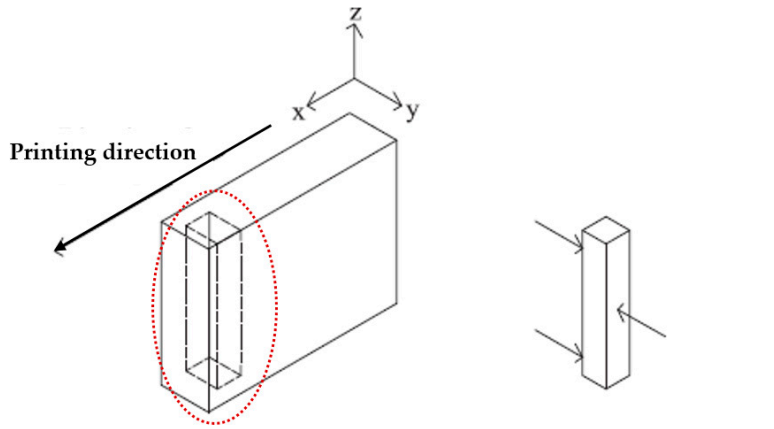
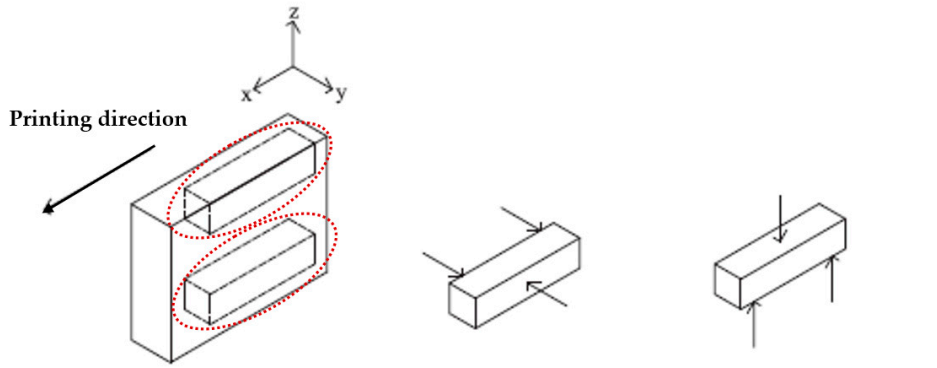


Figure 11. Beam slashed from the wall component for FS test [17].



(a) Extracting vertical beam from the wall element **(b) Loading direction E1**

Figure 12. Loading direction for vertically extracted beams [17].



(a) Extracting beam from the wall element **(b) Loading direction E2** **(c) Loading direction E3**

Figure 13. Loading direction for horizontally extracted beams [17].

5. Bibliometric Analysis

5.1. Methodology

The bibliometric analysis was performed via a detailed search of Scopus as the core collection database. The keyword utilised for searching was 3D print* concrete*. Subsequently, a comprehensive selection procedure was followed to manually check the downloaded publications based on their titles, keywords, and abstracts. In the process of sequential filtering, redundant topics in the literature were eliminated, thus only those related to 3DPC were considered. Eventually, 381 studies were chosen as the final dataset after filtering out publications related to the review paper. For the detailed analysis of the downloaded papers from the Scopus database, the freely available software VOSviewer (version 1.6.19) was used to generate various bibliometric maps based on the network data. This software provides distinctive features to the graphical portrayal of bibliometric mapping [79]. VOSviewer not only aims to analyse the bibliometric networks but can also generate, envisage, and discover diverse maps based on any kind of network data [65]. It can execute different kinds of analyses, such as co-authors, co-occurrences of keywords, and co-citations of cited journals/periodicals/authors/references. Additionally, the database of Scopus' central collection was utilised to produce the core data of yearly publications, statistics of citations, and types of documents that could illuminate the growth of 3D printable concrete over the years and the leading institutions in this particular subject area, respectively. Next, the original files extracted from Scopus were further managed in VOSviewer to envisage the bibliometric allocations by nation, referred resources, author index, and keywords co-occurrences.

5.2. Literature Samples

Figure 14 displays the annual increasing trend in the number of publications during 2016 to 2022. The first article on 3DPC was discovered in 2016. Thereafter, intense research interests were generated in the area of 3DPC. In addition, the number of publications in 2022 doubled based on the number of publications in the previous year. Hence, the number of publications has kept on continuously increasing over the years.

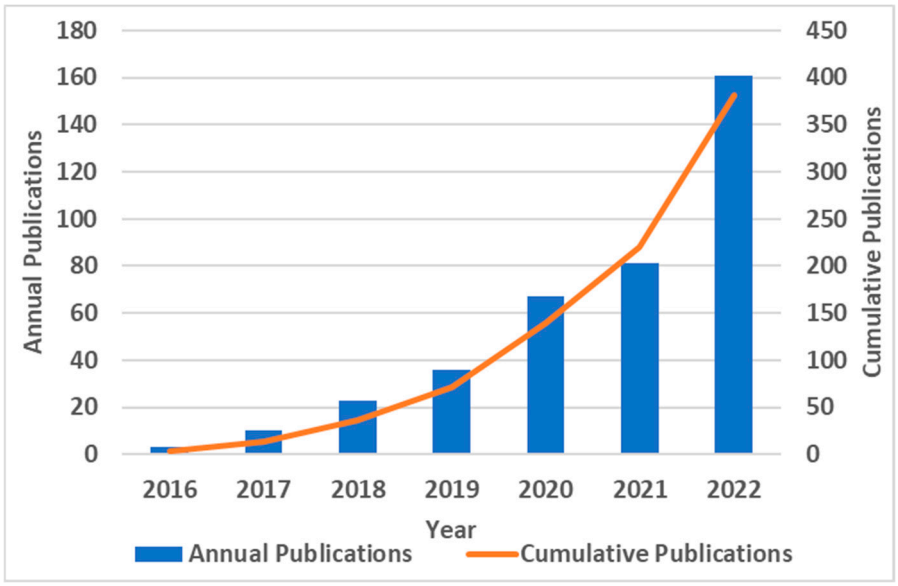


Figure 14. Annual and cumulative publications from 2016 to 2022.

5.3. Research Keywords

The main contents of any paper are defined through various keywords by the authors. Thus, the core area of any research domain can be understood by analysing the statistics related to the keywords that occur in the literature on a specific topic [80–83]. Table 4

displays the main keywords that appeared in the collected papers concerning 3DPC. The majority of the research emphasised three keywords, concrete, 3D printing, and 3DPC, which were the top listings. Figure 15 illustrates the co-occurrence of author keyword visualisation and their correlations depending on the strength of links. From a total of 943 keywords defined by various authors in their articles, only 95 were clustered in 15 groups, with different colours, which was achieved by setting the least occurrences at three and cleaning up of words. The frequency of occurrences of each term is reflected through its node size, wherein larger nodes signify a higher occurrence frequency of a term. The results reveal that in the field of 3DPC, the foremost keyword is 3DPC, which appears 185 times, with a total link strength of 305.

Table 4. Keywords used in the research articles.

S/N	Keyword	Occurrences	Total Link Strength
1	3D Printable Concrete	185	305
2	3D Printing	78	170
3	Concrete	48	118
4	Additive Manufacturing Technology	45	99
5	Mechanical Properties	35	70
6	Rheology	31	81
7	Buildability	24	56
8	Anisotropic Behaviour	17	40
9	Reinforcement	16	43
10	Durability	14	40
11	Interlayer Bonds	14	29
12	Compressive Strength	12	33
13	Microstructure	12	37
14	Printability	12	26
15	Pore Structure	11	30
16	Yield Stress	11	27
17	Sustainability	10	17
18	Workability	10	29
19	Porosity	9	27
20	Thixotropy	9	23
21	Flexural Strength	8	20
22	3D-Printed Concrete	7	10
23	Bond Strength	7	16
24	Digital Concrete	7	13
25	Digital Fabrication	7	13
26	Shrinkage	7	19
27	Rheological Properties	6	12
28	Accelerator	5	11
29	Cementitious Material	5	14
30	Coarse Aggregate	5	14
31	Finite Element Model Analysis	5	12
32	Fresh Properties	5	9

Table 4. *Cont.*

S/N	Keyword	Occurrences	Total Link Strength
33	Geopolymer	5	10
34	Interface	5	12
35	Shear Strength	5	7
36	Strength	5	13
37	Topology Optimisation	5	11
38	Bridge	4	12
39	Cable	4	16
40	Constructability	4	8
41	CSA Cement	4	9
42	Digital Image Correlation	4	7
43	Extrusion	4	11
44	Failure Mode	4	6
45	Finite Element	4	10
46	Finite Element Analysis	4	8
47	Fire Performance	4	8
48	Flowability	4	10
49	Fly Ash	4	10
50	Fresh Concrete	4	11

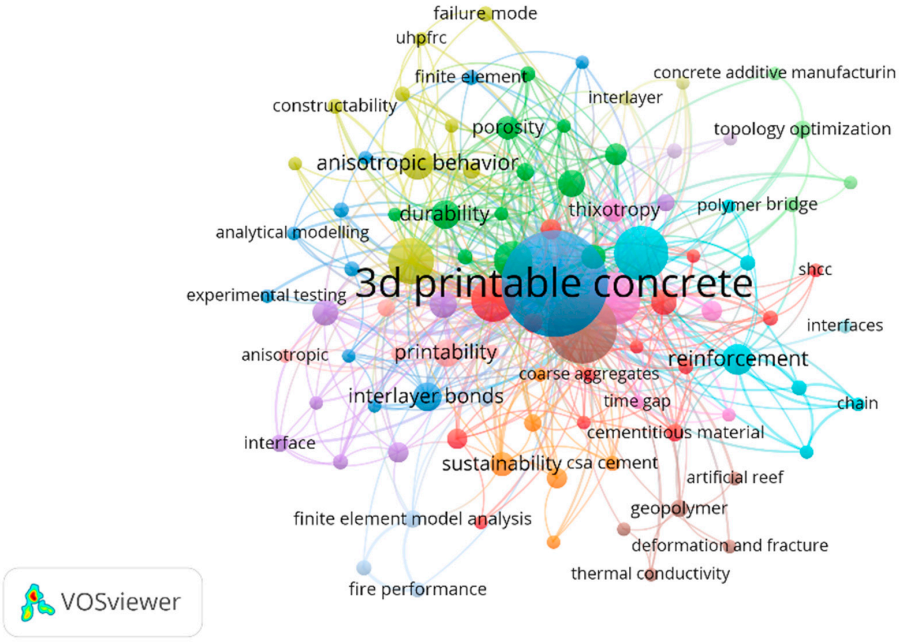


Figure 15. Visualisation of co-occurrence of author keywords.

5.4. Sources of Documents

Table 5 shows the number of documents published by various sources based on the research area of 3DPC. The journals *Construction and Building Materials* and *Rilem Bookseries* both ranked the highest regarding impact, with a total number of publications of 53 and 47, respectively. Figure 16 illustrates the annually published documents on 3DPC by source in the Scopus database during 2017 and 2022, indicating the prominence of the two journals in the field of 3DPC.

Table 5. Number of documents published by various sources.

Rank	Journal	No. of Publications	No. of Citations	Cite Score (2022)	The Most Cited Article	No. of Times Cited	Publisher
1	*Construction and Building Materials*	53 (13.9%)	1659	12.3	Effect of surface moisture on inter-layer strength of 3D-printed concrete	248	Elsevier
2	*Rilem Bookseries*	47 (12.3%)	253	1.6	Capillary water intake by 3DPC visualised and quantified by neutron radiography	30	Springer Nature
3	*Cement and Concrete Composites*	29 (7.6%)	671	15.4	3DPC: Mixture design and test methods	161	Elsevier
4	*Journal Of Building Engineering*	18 (4.7%)	131	8.2	Microstructural characterisation of 3D-printed concrete	26	Elsevier
5	*Materials*	18 (4.7%)	361	5.2	Experimental exploration of metal cable as reinforcement in 3DPC	102	Multidisciplinary Digital Publishing Institute (MDPI)

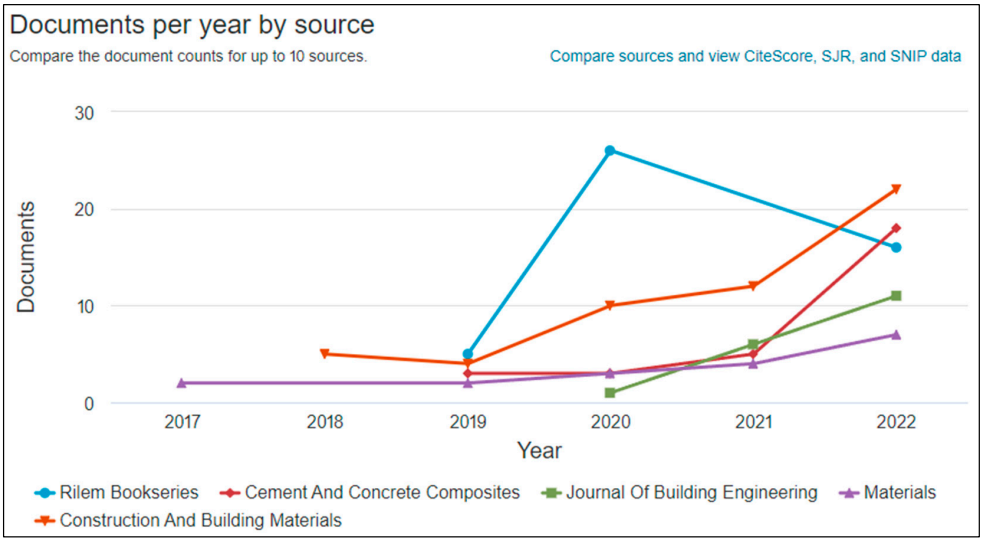


Figure 16. Number of documents by source per year.

5.5. Authors with Highest Citation

Table 6 shows various authors with the number of their publications and total citations in the field of 3DPC obtained from the Scopus database. The results show that 17 articles by Kruger, J. were cited 440 times, followed by more than 15 papers by De Schutter, G., Sanjayan, J., van Zijl, G., and Ma, Guowei. Among the 17 articles written by Kruger, J., 6 of them are about the weakness of 3DPC, such as porosity, plastic shrinkage cracking, interlayer bond strength, ductility, and behaviour in elevated temperatures, while 5 of them are about advanced 3DPC, such as steel reinforcement penetration, interlocking 3DPC, and buoyant foam concrete. The rest of the documents produced by Kruger, J. are about analytical modelling based on the characterisation of 3DPC. Figure 17 indicates the visualisation of authors with at least three published articles and links among the published papers and other authors based on the corporation during publication. In addition, the articles of Kruger, J. possess the largest node size, which represents he has the greatest number of publications.

Table 6. Authors with the total number of their publications and citations.

Rank	Author	Scopus Author ID	Year of 1st Publication	Total Publication	h-Index	Total Citation	Current Affiliation	Country
1	Kruger, J. [81,83–98]	57209803083	2019	17	15	440	Stellenbosch University, Stellenbosch, South Africa	South Africa
2	De Schutter, Geert D. [12,99–112]	7004339115	2018	15	57	457	Universiteit Gent, Ghent, Belgium	Belgium
3	Sanjayan, J. [113–128]	56094890900	2017	15	75	411	Swinburne University of Technology, Melbourne, Australia	Australia
4	van Zijl, Gideon P.A.G. [84–90,94–97,122–124,129–131]	6603009526	2019	15	27	363	Stellenbosch University, Stellenbosch, South Africa	South Africa
5	Ma, Guowei [125,126,132–144]	7202152174	2019	15	50	454	Hebei University of Technology, Tianjin, China	China
6	van Tittelboom, Kim [100–112,145]	34881161600	2020	14	33	73	Universiteit Gent, Ghent, Belgium	Belgium
7	Wang, Li [125,126,134–143,146,147]	57190428934	2019	14	28	406	Hebei University of Technology, Tianjin, China	China
8	Mechtcherine, Viktor [5,12,148–158]	15848808400	2018	13	58	538	Technische Universität Dresden, Dresden, Germany	Germany
9	Bos, Freek [11,14,159–167]	57190489675	2017	12	23	1112	Technical University of Munich, Munich, Germany	Germany
10	Rahul, A. V. [17,18,104–111,168,169]	57205203944	2019	12	12	354	Indian Institute of Technology Tirupati, Tirupati, India	India

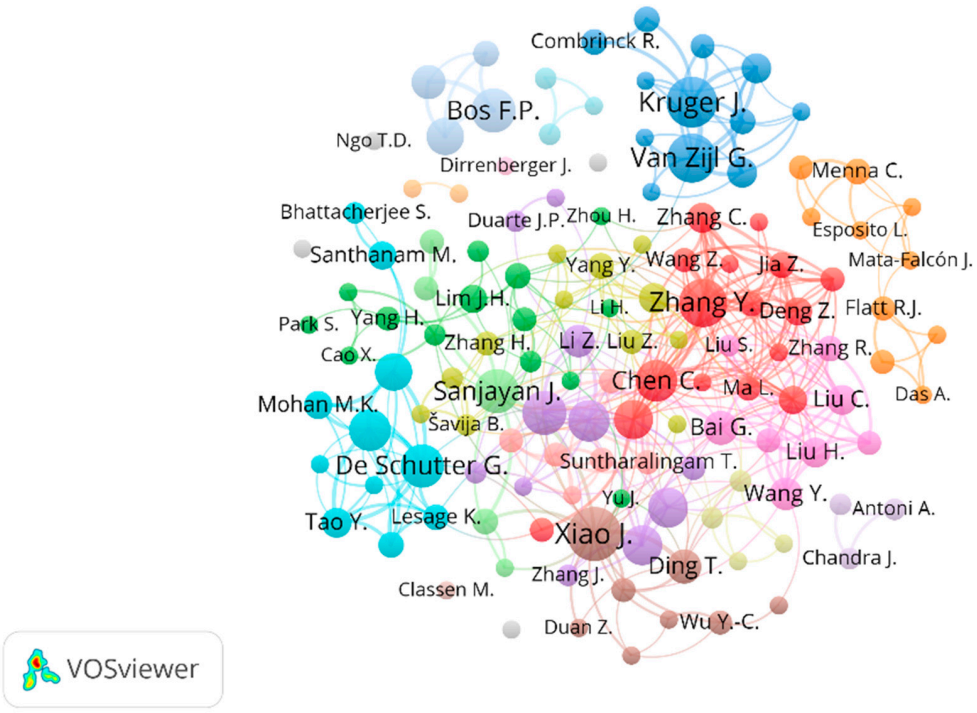


Figure 17. Visualisation of authors with at least 3 published articles.

5.6. Impact of Research Institutions

Table 7 shows the most contributing research institutions to the study of 3DPC extracted from the Scopus database. The Tongji University and Hebei University of Technology, located in China, occupy the first and second positions in the record rankings and have the strongest impact on 3DPC research, with 19 and 18 documents, respectively. The visualisation of research institutes (Figure 18) engaged in 3DPC studies disclosed that there is a need for continuous collaboration among various research institutes, as the highest total link strength is only 12 institutions, which are from Ghent University. Figure 19 illustrates the 10 most productive academic institutions in the area of 3DPC.

Table 7. Research institutions with the number of their publications and total citations.

S/N	Organisation	Documents	Citations	Total Link Strength
1	Tongji University	19	515	7
2	Hebei University of Technology	18	547	10
3	Eindhoven University of Technology	17	1399	10
4	Stellenbosch University	16	520	4
5	Ghent University	15	238	12
6	Swinburne University of Technology	13	693	3
7	Zhejiang University	13	68	7
8	Southeast University	12	561	10
9	Technische Universitat Dresden	11	590	5

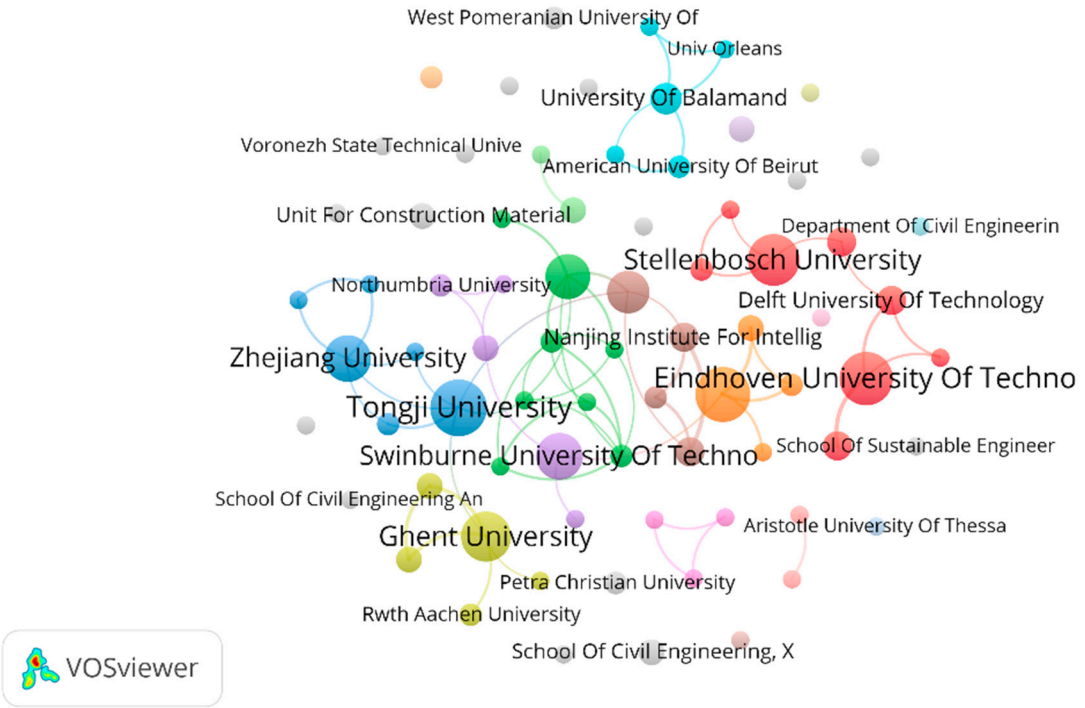


Figure 18. Visualisation of all related research institutions worldwide.



Figure 19. Top 10 most productive academic institutions in 3D printable concrete.

5.7. Countries

The overall bibliometric statistics related to co-authorships from various nations were analysed to ascertain the most prolific and prominent nations, together with their collaboration networks, in the field of 3DPC (Table 8). The results indicate the nations involved in conducting most of the research in 3DPC. Herein, China played a predominant role with 127 documents, followed by Australia, the United States, and South Africa with 38, 34, and 28 documents on 3DPC, respectively. In addition, China received the maximum citation count of 2050, making it the most contributing nation in the research domain of 3DPC. Figure 20 displays a combination of the document count per nation analysed by Scopus, crediting China with the maximum number of publications (127 articles) and Australia (38 papers) in second position. In essence, the contribution of China is identified in the sector of 3DPC in terms of quality and quantity viewpoints (Figure 21). This might be due to China having the highest number of documents with funding sponsors, as 75 studies are supported by the National Natural Science Foundation of China, as shown in Figure 22. The co-citation relationships among 37 nations through VOSviewer are clearly visualised. VOSviewer categorised 17 clusters in different colours through the collaboration network among all 36 countries. The occurrence of a link between two nations reveals that they had a collaboration, wherein a thicker link implies a stronger research collaboration in the development of 3DPC. The country that has the highest link strength is China with 53.

Table 8. Influential countries with the number of their publications and total citations.

S/N	Country	Documents	Citations	Total Link Strength
1	China	127	2050	53
2	Australia	38	1138	22
3	United States	34	232	14
4	South Africa	28	593	2

Table 8. *Cont.*

S/N	Country	Documents	Citations	Total Link Strength
5	Belgium	27	731	20
6	Netherlands	26	1603	8
7	Germany	25	658	22
8	France	20	711	26
9	India	17	369	4
10	United Kingdom	17	148	25
11	Singapore	14	510	15
12	Switzerland	14	646	11
13	Italy	11	57	9
14	South Korea	11	128	5
15	United Arab Emirates	8	39	0
16	Lebanon	7	118	7
17	Spain	7	57	12
18	Canada	6	73	6
19	Hong Kong	6	108	6
20	Poland	5	69	5
21	Portugal	5	51	10
22	Sri Lanka	5	45	8
23	Denmark	4	23	5
24	Greece	4	69	5
25	Indonesia	4	3	2
26	Colombia	3	1	1
27	Iran	3	85	3
28	Russian Federation	3	19	1
29	Saudi Arabia	3	8	5
30	Austria	2	15	2
31	Egypt	2	7	4
32	Estonia	2	22	3
33	French Polynesia	2	3	3
34	Ireland	2	7	2
35	Lithuania	2	33	1
36	Malaysia	2	113	3

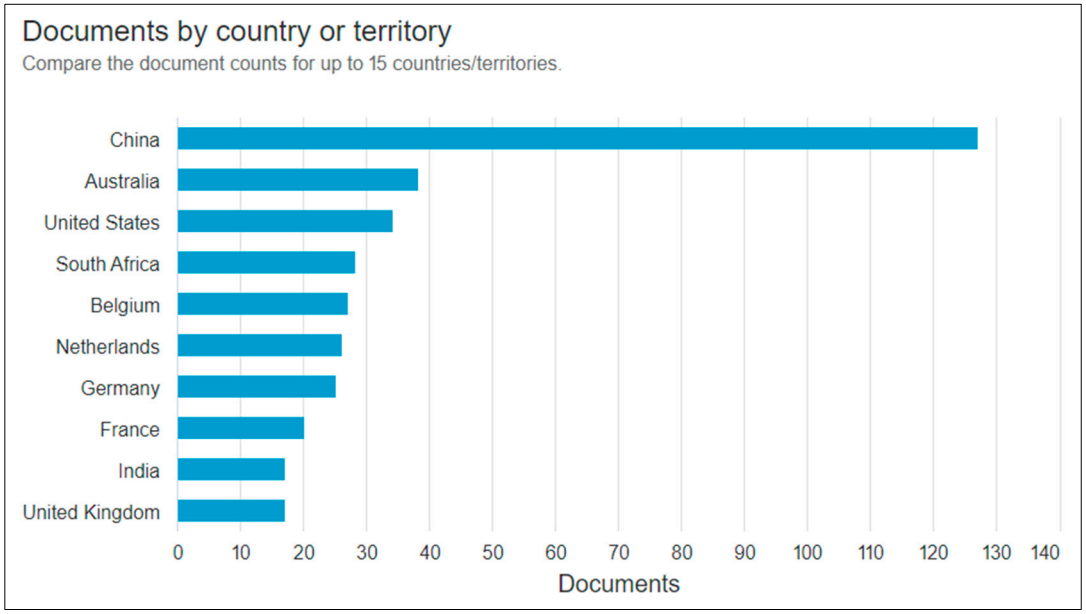


Figure 20. Document count per country.

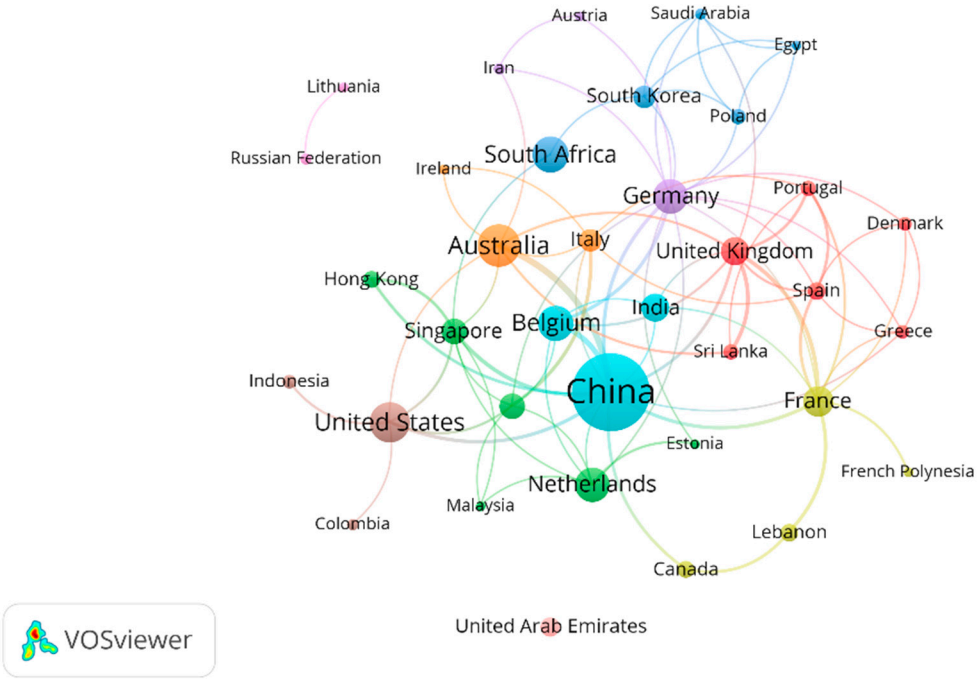


Figure 21. Visualisation of co-citation relationships among various nations.

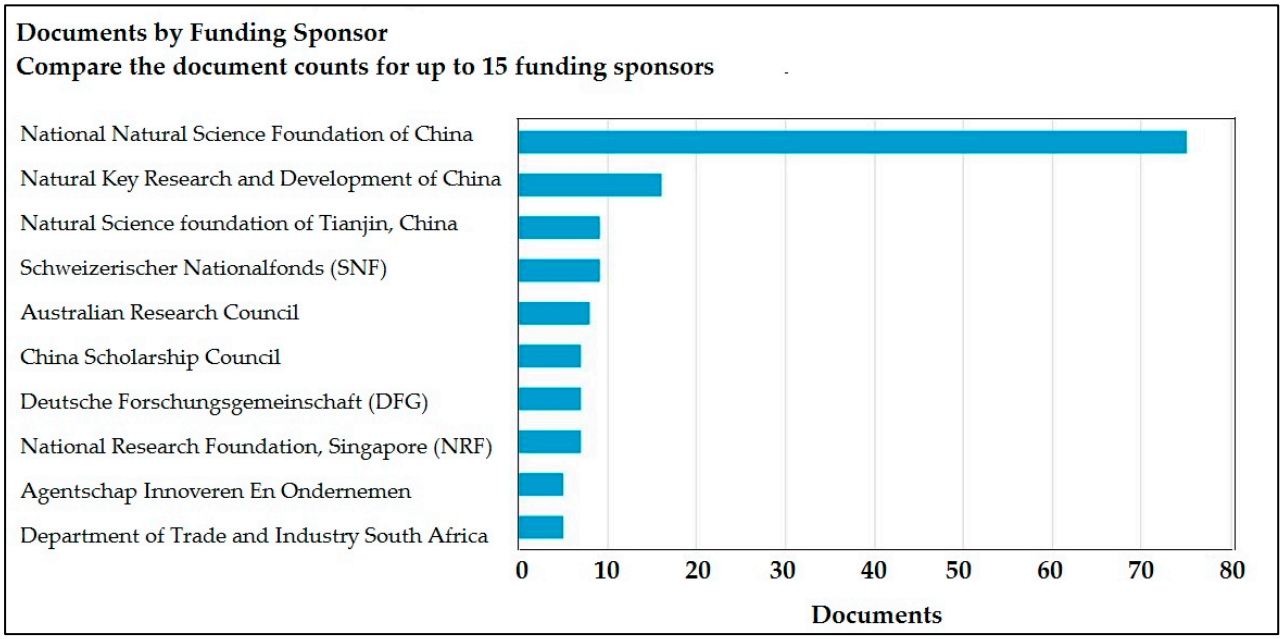


Figure 22. Documents for funding sponsor count.

6. Economic Considerations and Environmental Sustainability

Over the past decade, the cost of 3D-printed construction homes and structures has significantly decreased due to advancements in printable materials, reduced printer costs, the implementation of large-scale robotic printers, and the proliferation of specialised 3DPC companies [170]. However, it remains premature to calculate the ratio of 3DPC homes to conventionally cast concrete homes. One reason for this is the high cost of 3D-printed construction homes in most countries compared to alternative homes constructed with local materials and labour. Additionally, trust and awareness of 3DPC technology are still developing [4]. Currently, 3D-printed construction is not the only alternative to traditional concrete homes; there are other strong competitors that are rapidly gaining popularity. Notable examples include BOXABL foldable ready homes, TESLA tiny homes, and movable cabins (Figure 23) [4,170]. Although the low environmental impact of 3DPC is a significant advantage, other techniques offer equal or superior benefits in some cases, such as Tesla solar-roof homes [4].

It is well-known that sustainable technologies are characterised as self-sustaining initiatives aimed at enhancing overall quality of life with minimal compromise to current technological efficiency and cost-effectiveness [16,170]. The focus on sustainability has intensified within the construction industry, which accounts for about 40% of global energy consumption according to the 2019 Global Status Report for Buildings and Construction [170]. 3DPC has significant potential to reduce heavy dependence on natural resources and could establish a robust circular economy framework through the use of reusable materials and sustainable structural designs [4,19,170]. The Brundtland Commission (previously known as the World Commission on Environment and Development) divides sustainability into economic, social, and environmental dimensions [170]. Researchers in 3D printing construction (3DPC) have been promoting the use of industrial waste materials to achieve economic and environmental sustainability [6,170]. Operational efficiency can also be improved by reallocating manpower with the implementation of on-site automated 3DPC. Additionally, sources within the construction industry have highlighted the societal, economic, and environmental advantages of green buildings, which efficiently use natural resources (such as energy, water, materials, waste, toxicity, and air quality) throughout their lifecycle. However, studies on the practical implementation of sustainability in 3DPC are still scarce, as technical and procedural challenges persist.



Figure 23. 3D-printed construction applications of (**a**–**c**) Baxable Casita homes, (**d**–**f**) TESLA homes for sustainable living, and (**g**–**i**) energy-efficient buildings [4].

7. Conclusions

In conclusion, this review paper presents a comprehensive overview of various test procedures and mechanical characteristics of 3DPC made with different mix proportions. The paper highlights the need for the high mechanical strength and durability performance of 3DPC, which poses a new challenge in the construction sector. The review of the test methods and mechanical properties of 3DPC reveals that the bulk state of 3DPC is denser than mould-cast concrete, and the stress–strain relationship at early and late ages can be impacted by the displacement rate. Furthermore, the review shows that the overall attributes of 3DPC, especially the yield stress, are majorly decided by the mix proportion characteristics for deposit-wise stability, buildability, and extrudability in harnessing the technology.

The review also reveals that pumpability indicators, interfacial grades, and highest altitude printing can be used to evaluate the pumpability and buildability of 3DPC. The direct correlation between cement paste flowability and optimal aggregates in 3DPC was also discussed. The review further highlighted the importance of understanding the mechanical performance of 3D-printed wall components based on contact surface influence and porosity at the horizontal and vertical layers.

Overall, this review paper provides valuable insights into the current state of research on 3DPC and highlights the immense potential of this technology in the construction sector. The bibliometric analysis of research publications on 3DPC indicates an ever-increasing trend of research in this field, emphasising the need for continued research efforts to fully harness the potential of this technology. In conclusion, this review paper may serve as a taxonomy to navigate the field of 3DPC towards sustainable development.

8. Recommendations and Future Vision

Given the significant impact of process parameters on 3DPC processes, the development of monitoring systems for feedback applications appears essential for advancing automation in construction. Extensive research is required to fully implement fault diagnosis methods for 3DPC as a feedback system, necessitating a comprehensive understanding of the material, process, and feedback techniques.

Author Contributions: Conceptualisation, S.Q.T. and A.T.S.; methodology, S.Q.T. and N.H.A.S.L.; software, S.Q.T.; validation, G.F.H., A.T.S. and S.K.G.; formal analysis, S.Q.T.; investigation, A.T.S.; resources, N.H.A.S.L.; data curation, S.Q.T.; writing—original draft preparation, S.Q.T.; writing—review and editing, G.F.H. and S.K.G.; visualisation, A.T.S.; supervision, N.H.A.S.L.; project administration, A.T.S.; funding acquisition, G.F.H. and A.T.S. All authors have read and agreed to the published version of the manuscript.

Funding: This work was supported/funded by the Ministry of Higher Education under the Fundamental Research Grant Scheme R.J130000.7851.5F4261.

Data Availability Statement: Not applicable.

Acknowledgments: The authors thank Universiti Teknologi Malaysia for its support and cooperation in conducting this research.

Conflicts of Interest: The authors declare no conflicts of interest.

References

1. Martinez, S.; Balaguer, C.; Jardon, A.; Navarro, J.; Gimenez, A.; Barcena, C. Robotized lean assembly in the building industry. In Proceedings of the 25th International Symposium on Automation and Robotics in Construction, Vilnius, Lithuania, 26–29 June 2008.
2. Kazemian, A.; Yuan, X.; Cochran, E.; Khoshnevis, B. Cementitious materials for construction-scale 3D printing: Laboratory testing of fresh printing mixture. *Constr. Build. Mater.* **2017**, *145*, 639–647. [CrossRef]
3. Wohlers, T. Rapid prototyping & tooling state of the industry: 1998 worldwide progress report. *Mater. Technol.* **1998**, *13*, 174–176.
4. Ahmed, G.H. A review of "3D concrete printing": Materials and process characterization, economic considerations and environmental sustainability. *J. Build. Eng.* **2023**, *66*, 105863. [CrossRef]
5. Nerella, V.N.; Krause, M.; Mechtcherine, V. Direct printing test for buildability of 3D-printable concrete considering economic viability. *Autom. Constr.* **2020**, *109*, 102986. [CrossRef]
6. Wang, J.; Liu, Z.; Hou, J.; Ge, M. Research Progress and Trend Analysis of Concrete 3D Printing Technology Based on CiteSpace. *Buildings* **2024**, *14*, 989. [CrossRef]
7. Khoshnevis, B.; Hwang, D.; Yao, K.-T.; Yeh, Z. Mega-scale fabrication by contour crafting. *Int. J. Ind. Syst. Eng.* **2006**, *1*, 301–320. [CrossRef]
8. Khoshnevis, B.; Dutton, R. Innovative rapid prototyping process makes large sized, smooth surfaced complex shapes in a wide variety of materials. *Mater. Technol.* **1998**, *13*, 53–56. [CrossRef]
9. Khoshnevis, B. Automated construction by contour crafting—Related robotics and information technologies. *Autom. Constr.* **2004**, *13*, 5–19. [CrossRef]
10. Tay, Y.W.D.; Panda, B.; Paul, S.C.; Noor Mohamed, N.A.; Tan, M.J.; Leong, K.F. 3D printing trends in building and construction industry: A review. *Virtual Phys. Prototyp.* **2017**, *12*, 261–276. [CrossRef]
11. Wolfs, R.; Bos, F.; Salet, T. Early age mechanical behaviour of 3D printed concrete: Numerical modelling and experimental testing. *Cem. Concr. Res.* **2018**, *106*, 103–116. [CrossRef]
12. De Schutter, G.; Lesage, K.; Mechtcherine, V.; Nerella, V.N.; Habert, G.; Agusti-Juan, I. Vision of 3D printing with concrete—Technical, economic and environmental potentials. *Cem. Concr. Res.* **2018**, *112*, 25–36. [CrossRef]
13. Wangler, T.; Lloret, E.; Reiter, L.; Hack, N.; Gramazio, F.; Kohler, M.; Bernhard, M.; Dillenburger, B.; Buchli, J.; Roussel, N. Digital concrete: Opportunities and challenges. *RILEM Tech. Lett.* **2016**, *1*, 67–75. [CrossRef]
14. Bos, F.P.; Ahmed, Z.Y.; Wolfs, R.J.; Salet, T.A. 3D printing concrete with reinforcement. In *High Tech Concrete: Where Technology and Engineering Meet*; Springer: Berlin/Heidelberg, Germany, 2018; pp. 2484–2493.
15. Labonnote, N.; Rønnquist, A.; Manum, B.; Rüther, P. Additive construction: State-of-the-art, challenges and opportunities. *Autom. Constr.* **2016**, *72*, 347–366. [CrossRef]
16. Tu, H.; Wei, Z.; Alireza, B.; Nabil, B.K.; Ayaz, A.; Yasin, O.Ö. Recent advancements and future trends in 3D printing concrete using waste materials. *Dev. Built Environ.* **2023**, *16*, 100187. [CrossRef]
17. Rahul, A.; Santhanam, M.; Meena, H.; Ghani, Z. 3D printable concrete: Mixture design and test methods. *Cem. Concr. Compos.* **2019**, *97*, 13–23. [CrossRef]
18. Rahul, A.; Santhanam, M.; Meena, H.; Ghani, Z. Mechanical characterization of 3D printable concrete. *Constr. Build. Mater.* **2019**, *227*, 116710. [CrossRef]
19. Cheng, H.; Aleksandra, R.; Michael, H.; Liu, F.; Wang, J. Modeling concrete deposition via 3D printing using reproducing kernel particle method. *Cem. Concr. Res.* **2024**, *181*, 107526. [CrossRef]
20. Mueller, B. Additive manufacturing technologies–Rapid prototyping to direct digital manufacturing. *Assem. Autom.* **2012**, *32*, 1–12. [CrossRef]
21. Tay, Y.W.D.; Qian, Y.; Tan, M.J. Printability region for 3D concrete printing using slump and slump flow test. *Compos. Part B Eng.* **2019**, *174*, 106968. [CrossRef]

22. Parmigiani, S.; Devid, F.; Sandro, M.; Giuseppe, A.F.; Luciana, R. 3D-printed multi-functional foamed concrete building components: Material properties, component design, and 3D printing application. *Dev. Built Environ.* **2024**, *19*, 100483. [CrossRef]
23. Hasani, A.; Sattar, D. Transforming construction? Evaluation of the state of structural 3D concrete printing in research and practice. *Constr. Build. Mater.* **2024**, *438*, 137027. [CrossRef]
24. Lim, S.; Buswell, R.A.; Le, T.T.; Austin, S.A.; Gibb, A.G.; Thorpe, T. Developments in construction-scale additive manufacturing processes. *Autom. Constr.* **2012**, *21*, 262–268. [CrossRef]
25. Ramakrishnan, S.; Kirubajiny, P.; Viktor, M.; Jay, S. Printhead mixing of geopolymer and OPC slurries for hybrid alkali-activated cement in 3D concrete printing. *Constr. Build. Mater.* **2024**, *430*, 136439. [CrossRef]
26. Perkins, I.; Skitmore, M. Three-dimensional printing in the construction industry: A review. *Int. J. Constr. Manag.* **2015**, *15*, 1–9. [CrossRef]
27. Buswell, R.A.; Soar, R.C.; Gibb, A.G.; Thorpe, A. Freeform construction: Mega-scale rapid manufacturing for construction. *Autom. Constr.* **2007**, *16*, 224–231. [CrossRef]
28. Gosselin, C.; Duballet, R.; Roux, P.; Gaudillière, N.; Dirrenberger, J.; Morel, P. Large-scale 3D printing of ultra-high performance concrete–a new processing route for architects and builders. *Mater. Des.* **2016**, *100*, 102–109. [CrossRef]
29. Lloret, E.; Shahab, A.R.; Linus, M.; Flatt, R.J.; Gramazio, F.; Kohler, M.; Langenberg, S. Complex concrete structures: Merging existing casting techniques with digital fabrication. *Comput.-Aided Des.* **2015**, *60*, 40–49. [CrossRef]
30. Nerella, V.; Krause, M.; Näther, M.; Mechtcherine, V. 3D printing technology for on-site construction. *Concr. Plant Int.* **2016**, *4*, 36–41.
31. Buswell, R.A.; De Silva, W.L.; Jones, S.Z.; Dirrenberger, J. 3D printing using concrete extrusion: A roadmap for research. *Cem. Concr. Res.* **2018**, *112*, 37–49. [CrossRef]
32. De Schutter, G.; Feys, D. Pumping of fresh concrete: Insights and challenges. *RILEM Tech. Lett.* **2016**, *1*, 76–80. [CrossRef]
33. Feys, D.; Khayat, K.H.; Khatib, R. How do concrete rheology, tribology, flow rate and pipe radius influence pumping pressure? *Cem. Concr. Compos.* **2016**, *66*, 38–46. [CrossRef]
34. Mechtcherine, V.; Nerella, V.N.; Kasten, K. Testing pumpability of concrete using Sliding Pipe Rheometer. *Constr. Build. Mater.* **2014**, *53*, 312–323. [CrossRef]
35. Nerella, V.; Näther, M.; Iqbal, A.; Butler, M.; Mechtcherine, V. Inline quantification of extrudability of cementitious materials for digital construction. *Cem. Concr. Compos.* **2019**, *95*, 260–270. [CrossRef]
36. Jolin, M.; Burns, D.; Bissonnette, B.; Gagnon, F.; Bolduc, L.-S. Understanding the pumpability of concrete. In *Proceedings of the Shotcrete for Underground Support XI*; Engineering Conferences International; 2009; pp. 1–14. Available online: https://dc.engconfintl.org/shotcrete/17 (accessed on 21 August 2024).
37. Li, L.G.; Kwan, A.K. Mortar design based on water film thickness. *Constr. Build. Mater.* **2011**, *25*, 2381–2390. [CrossRef]
38. Li, L.G.; Kwan, A.K. Concrete mix design based on water film thickness and paste film thickness. *Cem. Concr. Compos.* **2013**, *39*, 33–42. [CrossRef]
39. Le, T.T.; Austin, S.A.; Lim, S.; Buswell, R.A.; Law, R.; Gibb, A.G.; Thorpe, T. Hardened properties of high-performance printing concrete. *Cem. Concr. Res.* **2012**, *42*, 558–566. [CrossRef]
40. Roussel, N.; Ovarlez, G.; Garrault, S.; Brumaud, C. The origins of thixotropy of fresh cement pastes. *Cem. Concr. Res.* **2012**, *42*, 148–157. [CrossRef]
41. Perrot, A.; Rangeard, D.; Pierre, A. Structural built-up of cement-based materials used for 3D-printing extrusion techniques. *Mater. Struct.* **2016**, *49*, 1213–1220. [CrossRef]
42. Marchon, D.; Kawashima, S.; Bessaies-Bey, H.; Mantellato, S.; Ng, S. Hydration and rheology control of concrete for digital fabrication: Potential admixtures and cement chemistry. *Cem. Concr. Res.* **2018**, *112*, 96–110. [CrossRef]
43. Roussel, N. *Understanding the Rheology of Concrete*; Elsevier: Amsterdam, The Netherlands, 2011.
44. Chadegani, A.A.; Salehi, H.; Yunus, M.M.; Farhadi, H.; Fooladi, M.; Farhadi, M.; Ebrahim, N.A. A comparison between two main academic literature collections: Web of Science and Scopus databases. *arXiv* **2013**, arXiv:1305.0377. [CrossRef]
45. Srinivasan, R.; DeFord, D.; Shah, S.P. The use of extrusion rheometry in the development of extruded fiber-reinforced cement composites. *Concr. Sci. Eng.* **1999**, *1*, 26–36.
46. Kuder, K.G.; Shah, S.P. Rheology of extruded cement-based materials. *ACI Mater. J.* **2007**, *104*, 283.
47. Tregger, N.A.; Pakula, M.E.; Shah, S.P. Influence of clays on the rheology of cement pastes. *Cem. Concr. Res.* **2010**, *40*, 384–391. [CrossRef]
48. Peled, A.; Cyr, M.F.; Shah, S.P. High content of fly ash (Class F) in extruded cementitious composites. *Mater. J.* **2000**, *97*, 509–517.
49. Voigt, T.; Mbele, J.-J.; Wang, K.; Shah, S.P. Using fly ash, clay, and fibers for simultaneous improvement of concrete green strength and consolidatability for slip-form pavement. *J. Mater. Civ. Eng.* **2010**, *22*, 196–206. [CrossRef]
50. Quanji, Z.; Lomboy, G.R.; Wang, K. Influence of nano-sized highly purified magnesium alumino silicate clay on thixotropic behavior of fresh cement pastes. *Constr. Build. Mater.* **2014**, *69*, 295–300. [CrossRef]
51. Heikal, M.; Ibrahim, N. Hydration, microstructure and phase composition of composite cements containing nano-clay. *Constr. Build. Mater.* **2016**, *112*, 19–27. [CrossRef]
52. Qian, Y.; De Schutter, G. Enhancing thixotropy of fresh cement pastes with nanoclay in presence of polycarboxylate ether superplasticizer (PCE). *Cem. Concr. Res.* **2018**, *111*, 15–22. [CrossRef]

53. Assaad, J.; Khayat, K.H.; Mesbah, H. Assessment of thixotropy of flowable and self-consolidating concrete. *Mater. J.* **2003**, *100*, 99–107.
54. Knapen, E.; Van Gemert, D. Cement hydration and microstructure formation in the presence of water-soluble polymers. *Cem. Concr. Res.* **2009**, *39*, 6–13. [CrossRef]
55. Yossef, M.; Chen, A. Applicability and limitations of 3D printing for civil structures. In Proceedings of the 2015 Conference on Autonomous and Robotic Construction of Infrastructure, Ames, IA, USA, 2–3 June 2015; pp. 237–246.
56. Ding, T.; Xiao, J.; Qin, F.; Duan, Z. Mechanical behavior of 3D printed mortar with recycled sand at early ages. *Constr. Build. Mater.* **2020**, *248*, 118654. [CrossRef]
57. Panda, B.; Lim, J.H.; Tan, M.J. Mechanical properties and deformation behaviour of early age concrete in the context of digital construction. *Compos. Part B Eng.* **2019**, *165*, 563–571. [CrossRef]
58. Hou, S.; Duan, Z.; Xiao, J.; Ye, J. A review of 3D printed concrete: Performance requirements, testing measurements and mix design. *Constr. Build. Mater.* **2021**, *273*, 121745. [CrossRef]
59. Makul, N. Advanced smart concrete—A review of current progress, benefits and challenges. *J. Clean. Prod.* **2020**, *274*, 122899. [CrossRef]
60. Moelich, G.M.; Kruger, J.; Combrinck, R. Plastic shrinkage cracking in 3D printed concrete. *Compos. Part B Eng.* **2020**, *200*, 108313. [CrossRef]
61. Tran, J.L. The law and 3D printing. *John Marshall J. Inf. Technol. Priv. Law* **2014**, *31*, 505.
62. Roussel, N. Rheological requirements for printable concretes. *Cem. Concr. Res.* **2018**, *112*, 76–85. [CrossRef]
63. Alghamdi, H.; Nair, S.A.O.; Neithalath, N. Insights into material design, extrusion rheology, and properties of 3D-printable alkali-activated fly ash-based binders. *Mater. Des.* **2019**, *167*, 107634. [CrossRef]
64. Le, T.T.; Austin, S.A.; Lim, S.; Buswell, R.A.; Gibb, A.G.; Thorpe, T. Mix design and fresh properties for high-performance printing concrete. *Mater. Struct.* **2012**, *45*, 1221–1232. [CrossRef]
65. Ma, G.; Li, Z.; Wang, L. Printable properties of cementitious material containing copper tailings for extrusion based 3D printing. *Constr. Build. Mater.* **2018**, *162*, 613–627. [CrossRef]
66. Lin, T.; Jia, D.; He, P.; Wang, M.; Liang, D. Effects of fiber length on mechanical properties and fracture behavior of short carbon fiber reinforced geopolymer matrix composites. *Mater. Sci. Eng. A* **2008**, *497*, 181–185. [CrossRef]
67. Austin, S.A.; Goodier, C.I.; Robins, P.J. Low-volume wet-process sprayed concrete: Pumping and spraying. *Mater. Struct.* **2005**, *38*, 229–237. [CrossRef]
68. *ASTM C109*; Standard Test Method for Compressive Strength of Hydraulic Cement Mortars (using 2-in. or [50-mm] cube specimens). American Society for Testing and Material: West Conshohocken, PA, USA, 2002; pp. 1–8.
69. *BS EN 12390-3*; Testing Hardened Concrete—Part 3: Compressive Strength of test Specimens. European Committee for Standardization-British Standard, 2009; pp. 1–18.
70. *ASTM C150*; Standard Specification for Portland Cement. American Society for Testing and Material: West Conshohocken, PA, USA, 2007; pp. 1–6.
71. *GB/T 50,081*; Standard for test methods of concrete physical and mechanical properties. Chinese Standard, 2002; pp. 1–7.
72. Zhang, Y.; Zhang, Y.; Liu, G.; Yang, Y.; Wu, M.; Pang, B. Fresh properties of a novel 3D printing concrete ink. *Constr. Build. Mater.* **2018**, *174*, 263–271. [CrossRef]
73. *ASTM C403*; Standard Test Method for Time of Setting of Concrete Mixtures by Penetration Resistance. American Society for Testing and Material: West Conshohocken, PA, USA, 2008; pp. 1–9.
74. *BS EN 196-9*; Methods of testing cement—Part 9: Heat of Hydration. European Committee for Standardization-British Standard, 2010; pp. 1–20.
75. *ASTM C230*; Standard Specification for Flow Table for Use in Tests of Hydraulic Cement. American Society for Testing and Material: West Conshohocken, PA, USA, 2020; pp. 1–6.
76. *ASTM C1437*; Standard Test Method for Flow of Hydraulic Cement Mortar. American Society for Testing and Material: West Conshohocken, PA, USA, 2020; pp. 1–9.
77. Casagrande, L.; Esposito, L.; Menna, C.; Asprone, D.; Auricchio, F. Effect of testing procedures on buildability properties of 3D-printable concrete. *Constr. Build. Mater.* **2020**, *245*, 118286. [CrossRef]
78. *ASTM C348*; Standard Test Method for Flexural Strength of Hydraulic-Cement Mortars. American Society for Testing and Material: West Conshohocken, PA, USA, 2021; pp. 1–7.
79. Van Eck, N.; Waltman, L. Software survey: VOSviewer, a computer program for bibliometric mapping. *Scientometrics* **2010**, *84*, 523–538. [CrossRef] [PubMed]
80. Boyack, K.W.; van Eck, N.J.; Colavizza, G.; Waltman, L. Characterizing in-text citations in scientific articles: A large-scale analysis. *J. Informetr.* **2018**, *12*, 59–73. [CrossRef]
81. Guo, Y.-M.; Huang, Z.-L.; Guo, J.; Li, H.; Guo, X.-R.; Nkeli, M.J. Bibliometric analysis on smart cities research. *Sustainability* **2019**, *11*, 3606. [CrossRef]
82. Wolfs, R.J.M.; Bos, F.P.; Salet, T.A.M. Triaxial compression testing on early age concrete for numerical analysis of 3D concrete printing. *Cem. Concr. Compos.* **2019**, *104*, 103344. [CrossRef]

83. Van den Heever, M.; du Plessis, A.; Bester, F.; Kruger, J.; van Zijl, G. A mechanistic evaluation relating microstructural morphology to a modified Mohr-Griffith compression-shear constitutive model for 3D printed concrete. *Constr. Build. Mater.* **2022**, *325*, 126743. [CrossRef]
84. Van den Heever, M.; du Plessis, A.; Kruger, J.; van Zijl, G. Evaluating the effects of porosity on the mechanical properties of extrusion-based 3D printed concrete. *Cem. Concr. Res.* **2022**, *153*, 106695. [CrossRef]
85. Kruger, J.; Cicione, A.; Bester, F.; Van den Heever, M.; Cho, S.; Walls, R.; and Van Zijl, G. Facilitating Ductile Failure of 3D Printed Concrete Elements in Fire. In Proceedings of the Second RILEM International Conference on Concrete and Digital Fabrication: Digital Concrete, Eindhoven, The Netherlands, 6–9 July 2020. RILEM Bookseries.
86. Kruger, J.; Mostert, J.-P.; and Van Zijl, G. A Strain-Based Constitutive Model Ensuring Aesthetic 3D Printed Concrete Structures: Limiting Differential Settlement of Filaments. In Proceedings of the RILEM International Conference on Concrete and Digital Fabrication, Loughborough, UK, 27–29 June 2022; RILEM Bookseries. pp. 1–10.
87. Kruger, J.; du Plessis, A.; van Zijl, G. An investigation into the porosity of extrusion-based 3D printed concrete. *Addit. Manuf.* **2021**, *37*, 101740. [CrossRef]
88. Kruger, J.; Zeranka, S.; van Zijl, G. 3D concrete printing: A lower bound analytical model for buildability performance quantification. *Autom. Constr.* **2019**, *106*, 102904. [CrossRef]
89. Kruger, J.; Zeranka, S.; van Zijl, G. An ab initio approach for thixotropy characterisation of (nanoparticle-infused) 3D printable concrete. *Constr. Build. Mater.* **2019**, *224*, 372–386. [CrossRef]
90. Kruger, J.; Zeranka, S.; van Zijl, G. A rheology-based quasi-static shape retention model for digitally fabricated concrete. *Constr. Build. Mater.* **2020**, *254*, 119241. [CrossRef]
91. Moelich, G.M.; Janse van Rensburg, J.J.; Kruger, J.; Combrinck, R. The Environment's Effect on the Interlayer Bond Strength of 3D Printed Concrete. In Proceedings of the RILEM International Conference on Concrete and Digital Fabrication, Loughborough, UK, 27–29 June 2022. RILEM Bookseries.
92. Moelich, G.M.; Kruger, J.; Combrinck, R. Modelling the interlayer bond strength of 3D printed concrete with surface moisture. *Cem. Concr. Res.* **2021**, *150*, 106559. [CrossRef]
93. Mostert, J.-P.; Kruger, J. Interlocking 3D Printed Concrete Filaments Through Surface Topology Modifications for Improved Tensile Bond Strength. In Proceedings of the RILEM International Conference on Concrete and Digital Fabrication, Loughborough, UK, 27–29 June 2022. RILEM Bookseries.
94. Bester, F.; Van den Heever, M.; Kruger, J.; Cho, S.; van Zijl, G. Steel Fiber Links in 3D Printed Concrete. In Proceedings of the Second RILEM International Conference on Concrete and Digital Fabrication: Digital Concrete, Eindhoven, The Netherlands, 6–9 July 2020. RILEM Bookseries.
95. Cho, S.; Kruger, J.; Bester, F.; Van den Heever, M.; Van Rooyen, A.; van Zijl, G. A Compendious Rheo-Mechanical Test for Printability Assessment of 3D Printable Concrete. In Proceedings of the Second RILEM International Conference on Concrete and Digital Fabrication: Digital Concrete, Eindhoven, The Netherlands, 6–9 July 2020. RILEM Bookseries.
96. Cho, S.; Kruger, J.; Van Rooyen, A.; van Zijl, G. Rheology and application of buoyant foam concrete for digital fabrication. *Compos. Part B Eng.* **2021**, *215*, 108800. [CrossRef]
97. Cho, S.; Van den Heever, M.; Kruger, J.; van Zijl, G. Proof-of-Concept: Sprayable SHCC Overlay Reinforcement Regime for Unreinforced 3D Printed Concrete Structure. In Proceedings of the RILEM International Conference on Concrete and Digital Fabrication, Loughborough, UK, 27–29 June 2022. RILEM Bookseries.
98. Cicione, A.; Kruger, J.; Walls, R.S.; Van Zijl, G. An experimental study of the behavior of 3D printed concrete at elevated temperatures. *Fire Saf. J.* **2021**, *120*, 103075. [CrossRef]
99. Jiao, D.; Shi, C.; De Schutter, G. Magneto-rheology control in 3D concrete printing: A rheological attempt. *Mater. Lett.* **2022**, *309*, 131374. [CrossRef]
100. Tao, Y.; Lesage, K.; Van Tittelboom, K.; Yuan, Y.; De Schutter, G. Influence of accelerator on the pore structure of 3D printable concrete. In Proceedings of the 2nd fib Italy YMG Symposium on Concrete and Concrete Structures, Roma, Italy, 18–19 November 2021; pp. 313–318.
101. Tao, Y.; Lesage, K.; Van Tittelboom, K.; Yuan, Y.; De Schutter, G. Influence of substrate surface roughness and moisture content on tensile adhesion performance of 3D printable concrete. *Cem. Concr. Compos.* **2022**, *126*, 104350. [CrossRef]
102. Tao, Y.; Ren, Q.; Lesage, K.; Van Tittelboom, K.; Yuan, Y.; De Schutter, G. Shape stability of 3D printable concrete with river and manufactured sand characterized by squeeze flow. *Cem. Concr. Compos.* **2022**, *133*, 104674. [CrossRef]
103. Tao, Y.; Lesage, K.; Van Tittelboom, K.; Yuan, Y.; De Schutter, G. Effect of Limestone Powder Substitution on Fresh and Hardened Properties of 3D Printable Mortar. In Proceedings of the Second RILEM International Conference on Concrete and Digital Fabrication: Digital Concrete, Eindhoven, The Netherlands, 6–9 July 2020. RILEM Bookseries.
104. Mohan, M.K.; Rahul, A.V.; De Schutter, G.; Van Tittelboom, K. Salt Scaling Resistance of 3D Printed Concrete. In Proceedings of the RILEM International Conference on Concrete and Digital Fabrication, Loughborough, UK, 27–29 June 2022. RILEM Bookseries.
105. Mohan, M.K.; Rahul, A.V.; Van Dam, B.; Zeidan, T.; De Schutter, G.; Van Tittelboom, K. Performance criteria, environmental impact and cost assessment for 3D printable concrete mixtures. *Resour. Conserv. Recycl.* **2022**, *181*, 106255. [CrossRef]
106. Tao, Y.; Rahul, A.V.; Lesage, K.; Van Tittelboom, K.; Yuan, Y.; De Schutter, G. Mechanical and microstructural properties of 3D printable concrete in the context of the twin-pipe pumping strategy. *Cem. Concr. Compos.* **2022**, *125*, 104324. [CrossRef]

107. Tao, Y.; Rahul, A.V.; Mohan, M.K.; Van Tittelboom, K.; Yuan, Y.; De Schutter, G. Blending performance of helical static mixer used for twin-pipe 3D concrete printing. *Cem. Concr. Compos.* **2022**, *134*, 104741. [CrossRef]
108. Rahul, A.V.; Mohan, M.K.; De Schutter, G.; Van Tittelboom, K. 3D printable concrete with natural and recycled coarse aggregates: Rheological, mechanical and shrinkage behaviour. *Cem. Concr. Compos.* **2022**, *125*, 104311. [CrossRef]
109. Mohan, M.K.; Rahul, A.V.; Van Tittelboom, K.; De Schutter, G. Evaluating the Influence of Aggregate Content on Pumpability of 3D Printable Concrete. In Proceedings of the Second RILEM International Conference on Concrete and Digital Fabrication: Digital Concrete, Eindhoven, The Netherlands, 6–9 July 2020. RILEM Bookseries.
110. Mohan, M.K.; Rahul, A.V.; De Schutter, G.; Van Tittelboom, K. Early age hydration, rheology and pumping characteristics of CSA cement-based 3D printable concrete. *Constr. Build. Mater.* **2021**, *275*, 122136. [CrossRef]
111. Mohan, M.K.; Rahul, A.V.; Tao, Y.; De Schutter, G.; Van Tittelboom, K. Hydration re-initiation of borated CSA systems with a two-stage mixing process: An application in extrusion-based concrete 3D printing. *Cem. Concr. Res.* **2022**, *159*, 106870. [CrossRef]
112. Ooms, T.; Vantyghem, G.; Tao, Y.; Bekaert, M.; De Schutter, G.; Van Tittelboom, K.; De Corte, W. The Production of a Topology-Optimized 3D-Printed Concrete Bridge. In Proceedings of the RILEM International Conference on Concrete and Digital Fabrication, Loughborough, UK, 27–29 June 2022. RILEM Bookseries.
113. Jayathilakage, R.I.; Rajeev, P.; Sanjayan, J. Predication of Strength-Based Failure in Extrusion-Based 3D Concrete Printing. In Proceedings of the Rheology and Processing of Construction Materials: RheoCon2 & SCC9, Dresden, Germany, 8–11 September 2019. RILEM Bookseries.
114. Jayathilakage, R.; Rajeev, P.; Sanjayan, J. Yield stress criteria to assess the buildability of 3D concrete printing. *Constr. Build. Mater.* **2020**, *240*, 117989. [CrossRef]
115. Jayathilakage, R.; Rajeev, P.; Sanjayan, J. Extrusion rheometer for 3D concrete printing. *Cem. Concr. Compos.* **2021**, *121*, 104075. [CrossRef]
116. Jayathilakage, R.; Sanjayan, J.; Rajeev, P. Direct shear test for the assessment of rheological parameters of concrete for 3D printing applications. *Mater. Struct.* **2019**, *52*, 12. [CrossRef]
117. Jayathilakage, R.; Sanjayan, J.; Rajeev, P. Characterizing Extrudability for 3D Concrete Printing Using Discrete Element Simulations. In Proceedings of the Second RILEM International Conference on Concrete and Digital Fabrication: Digital Concrete, Eindhoven, The Netherlands, 6–9 July 2020. RILEM Bookseries.
118. Muthukrishnan, S.; Ramakrishnan, S.; Sanjayan, J. Effect of alkali reactions on the rheology of one-part 3D printable geopolymer concrete. *Cem. Concr. Compos.* **2021**, *116*, 103899. [CrossRef]
119. Pham, L.; Tran, P.; Sanjayan, J. Steel fibres reinforced 3D printed concrete: Influence of fibre sizes on mechanical performance. *Constr. Build. Mater.* **2020**, *250*, 118785. [CrossRef]
120. Ramakrishnan, S.; Kanagasuntharam, S.; Sanjayan, J. In-line activation of cementitious materials for 3D concrete printing. *Cem. Concr. Compos.* **2022**, *131*, 104598. [CrossRef]
121. Xia, M.; Nematollahi, B.; Sanjayan, J. Influence of binder saturation level on compressive strength and dimensional accuracy of powder-based 3D printed geopolymer. *Mater. Sci. Forum* **2018**, *939*, 177–183. [CrossRef]
122. Xia, M.; Nematollahi, B.; Sanjayan, J.G. Properties of Powder-Based 3D Printed Geopolymers. In *3D Concrete Printing Technology: Construction and Building Applications*; Butterworth-Heinemann: Oxford, UK, 2019.
123. Yu, S.; Xia, M.; Sanjayan, J.; Yang, L.; Xiao, J.; Du, H. Microstructural characterization of 3D printed concrete. *J. Build. Eng.* **2021**, *44*, 102948. [CrossRef]
124. Nematollahi, B.; Bong, S.H.; Xia, M.; Sanjayan, J. Digital Fabrication of 'Just-Add-Water' Geopolymers: Effects of Curing Condition and Print-Time Interval. In Proceedings of the Second RILEM International Conference on Concrete and Digital Fabrication: Digital Concrete, Eindhoven, The Netherlands, 6–9 July 2020. RILEM Bookseries.
125. Bai, G.; Wang, L.; Ma, G.; Sanjayan, J.; Bai, M. 3D printing eco-friendly concrete containing under-utilised and waste solids as aggregates. *Cem. Concr. Compos.* **2021**, *120*, 104037. [CrossRef]
126. Li, Z.; Ma, G.; Wang, F.; Wang, L.; Sanjayan, J. Expansive cementitious materials to improve micro-cable reinforcement bond in 3D concrete printing. *Cem. Concr. Compos.* **2022**, *125*, 104304. [CrossRef]
127. Arunothayan, A.R.; Nematollahi, B.; Sanjayan, J.; Ranade, R.; Bong, S.H.; Khayat, K. Quantitative Evaluation of Orientation of Steel Fibers in 3D-Printed Ultra-High Performance Concrete. In Proceedings of the Second RILEM International Conference on Concrete and Digital Fabrication: Digital Concrete, Eindhoven, The Netherlands, 6–9 July 2020. RILEM Bookseries.
128. Marchment, T.; Xia, M.; Dodd, E.; Sanjayan, J.; Nematollahi, B. Effect of delay time on the mechanical properties of extrusion-based 3D printed concrete. In Proceedings of the ISARC 2017—34th International Symposium on Automation and Robotics in Construction, Taipei, Taiwan, 28 June–1 July 2017; pp. 240–245.
129. Christen, H.; van Zijl, G.; de Villiers, W. The incorporation of recycled brick aggregate in 3D printed concrete. *Clean. Mater.* **2022**, *4*, 100090. [CrossRef]
130. Christen, H.; Cho, S.; van Zijl, G.; de Villiers, W. Phase change material infused recycled brick aggregate in 3D printed concrete. *Heliyon* **2022**, *8*, e11598. [CrossRef] [PubMed]
131. Cho, S.; Van Rooyen, A.; Kearsley, E.; Van Zijl, G. Foam stability of 3D printable foamed concrete. *J. Build. Eng.* **2022**, *47*, 103884. [CrossRef]
132. Xiao, J.Z.; Liu, H.R.; Ding, T.; Ma, G.W. 3D printed concrete components and structures: An overview. *Sustain. Struct.* **2021**, *1*, 1–15. [CrossRef]

133. Sun, J.; Aslani, F.; Lu, J.; Wang, L.; Huang, Y.; Ma, G. Fibre-reinforced lightweight engineered cementitious composites for 3D concrete printing. *Ceram. Int.* **2021**, *47*, 27107–27121. [CrossRef]
134. Cui, T. Effect of HB-CSA and Expansion Agent on Shrinkage and Cracking Performance of 3D Printing Concret. *Cailiao Daobao/Mater. Rep.* **2022**, *36*, 80–86.
135. Wang, L.; Ma, G.; Liu, T.; Buswell, R.; Li, Z. Interlayer reinforcement of 3D printed concrete by the in-process deposition of U-nails. *Cem. Concr. Res.* **2021**, *148*, 106535. [CrossRef]
136. Wang, L.; Xiao, W.; Wang, Q.; Jiang, H.; Ma, G. Freeze-thaw resistance of 3D-printed composites with desert sand. *Cem. Concr. Compos.* **2022**, *133*, 104693. [CrossRef]
137. Wang, L.; Tian, Z.; Ma, G.; Zhang, M. Interlayer bonding improvement of 3D printed concrete with polymer modified mortar: Experiments and molecular dynamics studies. *Cem. Concr. Compos.* **2020**, *110*, 103571. [CrossRef]
138. Ma, G.; Li, Z.; Wang, L.; Bai, G. Micro-cable reinforced geopolymer composite for extrusion-based 3D printing. *Mater. Lett.* **2019**, *235*, 144–147.
139. Li, Z.; Wang, L.; Ma, G. Mechanical improvement of continuous steel microcable reinforced geopolymer composites for 3D printing subjected to different loading conditions. *Compos. Part B Eng.* **2020**, *187*, 107796. [CrossRef]
140. Bai, G.; Wang, L.; Wang, F.; Ma, G. In-process reinforcing method: Dual 3D printing procedure for ultra-high performance concrete reinforced cementitious composites. *Mater. Lett.* **2021**, *304*, 130594. [CrossRef]
141. Wang, L.; Yang, Y.; Yao, L.; Ma, G. Interfacial bonding properties of 3D printed permanent formwork with the post-casted concrete. *Cem. Concr. Compos.* **2022**, *128*, 104457. [CrossRef]
142. Liu, M.; Zhang, Q.; Tan, Z.; Wang, L.; Li, Z.; Ma, G. Investigation of steel wire mesh reinforcement method for 3D concrete printing. *Arch. Civ. Mech. Eng.* **2021**, *21*, 24. [CrossRef]
143. Ma, G.; Salman, N.M.; Wang, L.; Wang, F. A novel additive mortar leveraging internal curing for enhancing interlayer bonding of cementitious composite for 3D printing. *Constr. Build. Mater.* **2020**, *244*, 118305. [CrossRef]
144. Sun, J.; Huang, Y.; Aslani, F.; Ma, G. Properties of a double-layer EMW-absorbing structure containing a graded nano-sized absorbent combing extruded and sprayed 3D printing. *Constr. Build. Mater.* **2020**, *261*, 120031. [CrossRef]
145. Saelens, L.; Van Tittelboom, K.; Caspeele, R.; Wan-Wendner, R. Topology optimization of structural beam systems considering 3D concrete printing technology constraints. In Proceedings of the 4th International PhD Symposium in Civil Engineering, Rome, Italy, 5–7 September 2022; Volume 58, pp. 825–832.
146. Wang, L.; Liu, Y.; Yang, Y.; Li, Y.; Bai, M. Bonding performance of 3D printing concrete with self-locking interfaces exposed to compression–shear and compression–splitting stresses. *Addit. Manuf.* **2021**, *42*, 101992. [CrossRef]
147. Wang, L.; Lin, W.; Ma, H.; Li, D.; Wang, Q. Mechanical and microstructural properties of 3D-printed aluminate cement based composite exposed to elevated temperatures. *Constr. Build. Mater.* **2022**, *353*, 129144. [CrossRef]
148. Zhang, C.; Hou, Z.; Chen, C.; Zhang, Y.; Mechtcherine, V.; Sun, Z. Design of 3D printable concrete based on the relationship between flowability of cement paste and optimum aggregate content. *Cem. Concr. Compos.* **2019**, *104*, 103406. [CrossRef]
149. Zhang, C.; Jia, Z.; Wang, X.; Jia, L.; Deng, Z.; Wang, Z.; Zhang, Y.; Mechtcherine, V. A two-phase design strategy based on the composite of mortar and coarse aggregate for 3D printable concrete with coarse aggregate. *J. Build. Eng.* **2022**, *54*, 104672. [CrossRef]
150. Zhang, C.; Deng, Z.; Chen, C.; Zhang, Y.; Mechtcherine, V.; Sun, Z. Predicting the static yield stress of 3D printable concrete based on flowability of paste and thickness of excess paste layer. *Cem. Concr. Compos.* **2022**, *129*, 104494. [CrossRef]
151. Liu, H.; Ding, T.; Xiao, J.; Mechtcherine, V. Buildability prediction of 3D–printed concrete at early-ages: A numerical study with Drucker–Prager model. *Addit. Manuf.* **2022**, *55*, 102821. [CrossRef]
152. Markin, S.; Mechtcherine, V. Measuring Plastic Shrinkage and Related Cracking of 3D Printed Concretes. In Proceedings of the RILEM International Conference on Concrete and Digital Fabrication, Loughborough, UK, 27–29 June 2022. RILEM Bookseries.
153. Schröfl, C.; Nerella, V.N.; Mechtcherine, V. Capillary water intake by 3D-printed concrete visualised and quantified by neutron radiography. In *First RILEM International Conference on Concrete and Digital Fabrication–Digital Concrete 2018*; Springer: Berlin/Heidelberg, Germany, 2019; RILEM Bookseries.
154. Ghourchian, S.; Butler, M.; Krüger, M.; Mechtcherine, V. Modelling the development of capillary pressure in freshly 3D-printed concrete elements. *Cem. Concr. Res.* **2021**, *145*, 106457. [CrossRef]
155. Taubert, M.; Mechtcherine, V. Mix Design for a 3D-Printable Concrete with Coarse Aggregates and Consideration of Standardisation. In Proceedings of the RILEM International Conference on Concrete and Digital Fabrication, Loughborough, UK, 27–29 June 2022. RILEM Bookseries.
156. Mechtcherine, V.; Nerella, V.N.; Ogura, H.; Grafe, J.; Spaniol, E.; Hertel, M.; Füssel, U. Alternative reinforcements for digital concrete construction. In *First RILEM International Conference on Concrete and Digital Fabrication–Digital Concrete 2018*; Springer: Berlin/Heidelberg, Germany, 2019; RILEM Bookseries.
157. Reißig, S.; Nerella, V.N.; Mechtcherine, V. Material Design and Rheological Behavior of Sustainable Cement-Based Materials in the Context of 3D Printing. In Proceedings of the RILEM International Conference on Concrete and Digital Fabrication, Loughborough, UK, 27–29 June 2022. RILEM Bookseries.
158. Neef, T.; Müller, S.; Mechtcherine, V. Integration of Mineral Impregnated Carbon Fibre (MCF) into Fine 3D-Printed Concrete Filaments. In Proceedings of the RILEM International Conference on Concrete and Digital Fabrication, Loughborough, UK, 27–29 June 2022. RILEM Bookseries.

159. Costanzi, C.B.; Ahmed, Z.Y.; Schipper, H.R.; Bos, F.P.; Knaack, U.; Wolfs, R.J.M. 3D Printing Concrete on temporary surfaces: The design and fabrication of a concrete shell structure. *Autom. Constr.* **2018**, *94*, 395–404. [CrossRef]
160. Hass, L.; Bos, F.P.; Salet, T.A.M. Characterizing the bond properties of automatically placed helical reinforcement in 3D printed concrete. *Constr. Build. Mater.* **2022**, *355*, 129228. [CrossRef]
161. Wolfs, R.J.M.; Bos, F.P.; Salet, T.A.M. Correlation between destructive compression tests and non-destructive ultrasonic measurements on early age 3D printed concrete. *Constr. Build. Mater.* **2018**, *181*, 447–454. [CrossRef]
162. Wolfs, R.J.M.; Bos, F.P.; Salet, T.A.M. Hardened properties of 3D printed concrete: The influence of process parameters on interlayer adhesion. *Cem. Concr. Res.* **2019**, *119*, 132–140. [CrossRef]
163. Salet, T.A.; Ahmed, Z.Y.; Bos, F.P.; Laagland, H.L. 3D printed concrete bridge. In Proceedings of the International Conference on Progress in Additive Manufacturing, Singapore, 14–17 May 2018; pp. 2–9.
164. Salet, T.A.; Ahmed, Z.Y.; Bos, F.P.; Laagland, H.L. Design of a 3D printed concrete bridge by testing. *Virtual Phys. Prototyp.* **2018**, *13*, 222–236. [CrossRef]
165. Bos, F.P.; Ahmed, Z.Y.; Jutinov, E.R.; Salet, T.A. Experimental exploration of metal cable as reinforcement in 3D printed concrete. *Materials* **2017**, *10*, 1314. [CrossRef]
166. Bos, F.P.; Bosco, E.; Salet, T.A.M. Ductility of 3D printed concrete reinforced with short straight steel fibers. *Virtual Phys. Prototyp.* **2019**, *14*, 160–174. [CrossRef]
167. Ahmed, Z.Y.; Bos, F.P.; Van Brunschot, M.C.A.J.; Salet, T.A. On-demand additive manufacturing of functionally graded concrete. *Virtual Phys. Prototyp.* **2020**, *15*, 194–210. [CrossRef]
168. Bhattacherjee, S.; Basavaraj, A.S.; Rahul, A.V.; Santhanam, M.; Gettu, R.; Panda, B.; Schlangen, E.; Chen, Y.; Copuroglu, O.; Ma, G.; et al. Sustainable materials for 3D concrete printing. *Cem. Conc. Composites. J.* **2021**, *122*, 104156. [CrossRef]
169. Rahul, A.V.; Santhanam, M. Evaluating the printability of concretes containing lightweight coarse aggregates. *Cem. Concr. Compos.* **2020**, *109*, 103570. [CrossRef]
170. Quah, T.K.N.; Yi, W.D.T.; Jian, H.L.; Ming, J.T.; Teck, N.W.; King, H.H.L. Concrete 3D printing: Process parameters for process control, monitoring and diagnosis in automation and construction. *Mathematics* **2023**, *11*, 1499. [CrossRef]

Disclaimer/Publisher's Note: The statements, opinions and data contained in all publications are solely those of the individual author(s) and contributor(s) and not of MDPI and/or the editor(s). MDPI and/or the editor(s) disclaim responsibility for any injury to people or property resulting from any ideas, methods, instructions or products referred to in the content.